part of an alpha helix (Figure 2), but is not conserved in other A3 domains (Figure 1). In A3A, this region is completely missing, while in A3C, A3G-CTD, and A3F-CTD, there is a loss of four (A3C, A3G-CTD) or two (A3F-CTD) basic residues. Deletion of A3H residues R20, R21, and P22 (the del(20–22) mutant) results in significant loss, but not complete abolition of deaminase activity (Figure 4C), possibly due to perturbation of the local structure in the mutant protein. Although this mutant is efficiently packaged into virions (Figure 5A), it cannot restrict HIV-1 (Figure 5B).

Residues in A3H that are unique to its Z3 domain e.g., T81 and V135 are replaced in other active deaminase domains by S and I respectively, which are chemically similar (Figure 1 and Additional file 1: Figure S1). This implies similarity in function and is consistent with our finding that the A3H mutants T81S and V135I, retain enzymatic (Figure 4B and E, respectively) as well as restriction activity (Figure 5C). However, the T81A mutant in which the hydroxyl group common to T and S, is removed, has only background levels of deaminase activity (Figure 4B). This suggests an important structural role for the hydroxyl group at this position, possibly participation in hydrogen bonding interactions with a nearby side chain. In fact, the Oγ atom of S284, the corresponding residue in A3G, is within hydrogen bonding distance to the Y219 H_N backbone atom and is also observed in other A3 proteins [41,43,49,54]. It is interesting that despite lacking enzymatic activity, the T81A mutant exhibits significant antiviral activity (Figure 5D).

Although the loop 7 element of A3 proteins plays an essential role in determining deaminase specificity, each protein possesses a unique sequence (Figure 1) and is affected differently when subjected to mutation. For example, as indicated by modeling the A3A/ssDNA complex, the A3A loop 7 cluster of residues (127-ARI**Y-DYD**PL-135) interacts with the T (D133) and A (D131, Y132, and D133) nucleotides in the T**C**A motif, while D131 makes contacts with the central C [41]. Substitutions in all four cluster residues lead to complete loss of A3A deaminase activity [42]. In the case of the A3G-CTD loop 7 (313-RI**YDDQ**GR-320), mutation of the only aromatic residue, Y315, negatively impacts deaminase activity [43]. Additionally, changing both D316 and D317 to R [43] or replacing D317 with the corresponding A3A residue (Y132) [46] results in altered deaminase substrate specificity, as manifested by preferential deamination of the central C in the motif C**C**C instead of the 3′ C (CC**C**). Exchanging the A3H loop 7 (109-SRL**YYHW**CK-118) cluster residues YHW with the corresponding A3G-CTD residues, DDQ (YYHW→YDDQ), abrogates deamination activity (Figure 4E). This could reflect a change in substrate specificity or in the details of the nucleic acid binding mode due to a protein conformational change. Interestingly, a similar switch in sequence in the case of A3A (YDYD→YDDD) also reduces activity to background levels [42].

The importance of the A3H W115 residue in loop 7 is underscored by our finding that mutation of W115 to A results in low cellular protein levels (Figures 4D and 5A), blocks packaging into virions (Figure 5A), and eliminates deaminase (Figure 4F) and antiviral (Figure 5B) activities. Wang et al. [29] were unable to detect expression of (Hap VII) W115A in 293T cells, while Zhen et al. [57] reported that (Hap II) W115A is present at low levels in cell lysates. However, even when expression is equivalent to that of WT (by transfecting cells with a high amount of the Hap II mutant plasmid), W115A is barely detectable in viral lysates, does not restrict HIV-1, and binds cellular RNAs with greatly reduced efficiency [57]. Collectively, these results lend further support to the conclusion that the identity of loop 7 residues is critical for enzyme function.

Surprisingly, although A3H is highly basic and has only one domain, it more closely resembles the double-domain proteins A3D, A3F, and A3G than the single-domain A3A and A3C proteins with respect to several important biological properties. For example, like A3D, A3F, and A3G [53,64,82-92], A3H associates in solution in the absence of nucleic acid [93] and forms multimers and high molecular weight ribonucleoprotein complexes in cells [92,94]. In addition, it restricts the infectivity of HIV-1*vif* (–) virions (Figure 5) [26,27,62,80,94]. The anti-HIV-1 activity of A3 proteins A3D, A3F, A3G, and A3H involves (i) packaging of the proteins into the cores of nascent virions in the producer cell [28,36,95,96]; and (ii) inhibition of viral replication in the target cell (reviewed in ref. [9]). These parameters are linked to subcellular localization, which varies among the A3 proteins. However, in this case too, just as A3D, A3F, and A3G are located in the cytoplasm [82-84,86,92,97-99], A3H haplotypes that have antiviral activity (e.g., Hap II) are predominantly cytoplasmic [28,100].

The packaging of antiviral A3 proteins inside the HIV-1 core allows them to interact directly with viral nucleic acids (genomic RNA and nascent DNA synthesized during reverse transcription) in the presence of nucleocapsid protein and reverse transcriptase (RT). Here we show that A3H inhibits viral infectivity by both deaminase-dependent and -independent mechanisms (Figure 5), although it is likely that deaminase-dependent activity is dominant (compare data for WT and the catalytic mutant E56A in Figure 5D, Figure 6, Additional file 4: Figure S4). For A3G, we have proposed a "roadblock" mechanism that is based on its tight nucleic acid binding [61,101] and that is independent of catalytic activity [69,74]. We reasoned that since A3G displays slow on-off binding kinetics [69,79], RT is unable to traverse the

template when A3G is bound and consequently, RT-catalyzed polymerization is blocked. Recent single molecule stretching studies in support of this mechanism showed that A3G can transform from a fast enzyme (required for deamination) to a slow enzyme (causing a roadblock) during the course of protein oligomerization [79].

The highly basic character of the A3H protein (Figure 2B, Table 1) (like the NTDs of A3D, A3F, and A3G) strongly suggests that it also binds tightly to viral RNA and DNA, in agreement with studies of A3H binding to cellular RNA [57]. Moreover, the observed reduction in minus- and plus-strand DNA synthesis by RT, even in the absence of deaminase activity (Figure 6) and the fact that A3H can multimerize [92,93] suggest that a roadblock mechanism might also be relevant to A3H deaminase-independent HIV-1 restriction (Figure 6). Interestingly, although A3H mediates hypermutation of HIV-1 [27,48,62] and HBV [17] DNA, the antiviral activity of A3H against HTLV-1 does not involve editing [15].

In summary, A3H as well as A3D, A3F, and A3G constitute a group of A3 proteins used by the human innate immune system in its arsenal against HIV-1. The selective pressure to maintain expression of antiviral haplotypes of A3H in certain populations warrants greater understanding of this protein in terms of its molecular properties. Here, we present such an analysis and correlate enzyme function and antiviral activity. Although A3H is a single-domain protein and the most divergent member of the A3 family, we show that it utilizes strategies similar to those used by other antiviral double-domain A3 proteins (A3D, A3F, and A3G) to counteract HIV-1 infectivity. Knowledge of A3H structure-function relationships should be invaluable for the design of drugs to modulate A3H deaminase activity and augment its anti-HIV effect. Furthermore, since A3H is a single-domain protein and contains a unique Z3 domain, it may present a more specific target than the double-domain antiviral A3 proteins. Thus, taken together, A3H clearly provides a molecular paradigm to explore the antiviral response of A3 proteins to retroviral pathogens.

Conclusions

Based on a homology model of A3H Hap II and the results of extensive mutagenesis, we have identified structural elements and key residues associated with A3H deaminase and anti-HIV-1 activities. In addition, we provide evidence that A3H restriction of HIV-1 replication and inhibition of reverse transcription occur by deaminase-dependent and -independent mechanisms.

Methods

Materials

DNA oligonucleotides labeled with AlexaFluor 488® were obtained from Integrated DNA Technologies (Coralville, IA). The concentration of each oligonucleotide was determined by measuring its absorbance at 260 nm, using the extinction coefficients provided by the manufacturer. RNase A (endonuclease-free) was purchased from Qiagen Inc. (Germantown, MD). *Escherichia coli* uracil DNA glycosylase (UDG) was obtained from New England Biolabs (Beverly, MA). Gel loading buffer and nuclease-free water were purchased from Ambion® (Life Technologies, Grand Island, NY). Anti-A3H sera (p3A3 or p1H6), anti-HIV-1 CA sera (for ERT experiments), and TZM-bl cells (from John C. Kappes, Xiaoyun Wu, and Tranzyme Inc.) [102-104] were obtained from the AIDS Research and Reference Reagent Program (Division of AIDS, NIAID, NIH). An anti-HIV-1 p24 monoclonal antibody was purchased from ZeptoMetrix (Franklin, MA) and was used for detection of CA and $Pr55^{gag}$ in virions and cell lysates, respectively (see Figure 5). A monoclonal antibody (Anti-FLAG M2) against a FLAG tag was obtained from Sigma-Aldrich (St. Louis, MO). Anti-tubulin antibody was purchased from Abcam (Cambridge, MA).

Construction of the A3H HapII homology model

The initial A3H Hap II homology model was constructed without a Zn atom and was based on the A3G-CTD crystal structure (PDB: 3IR2) [53] by using MODELLER version 9v8 [56] and the sequence alignment shown in Figure 1. The Zn atom was subsequently added to the structure at a position equivalent to that in the structure of A3G-CTD. This was followed by energy minimization where only the Zn ion and the H54, C85, C88 side-chains were allowed to move. During the energy minimization, the lengths of the coordination bonds were kept as follows: 1.90 Å for the bond between the Zn ion and the H54 $N_{\delta 1}$ atom; and 2.25 Å for the bond between the Zn ion and the C85 or C88 S_γ atom. The charge of individual atoms and their radius parameters based on an amber force field [105] were generated by the pdb2pqr program [106]. Partial charges of atoms within the Zn coordination site were manually adjusted to +1e for the Zn ion, –0.6e for the S_γ atom and +0.1e for the C_β atom of the cysteines to account for the approximate redistribution of the charges between the two reduced cysteines and Zn ion through the coordination bonds. All structure and electrostatic potential map figures were generated with MOLMOL [107]. Sequence identity was determined with DNAStar (http://www.dnastar.com/megalign_help/index.html#!Documents/calculationofpercent.htm).

Construction of A3H mutants

pTR600 mammalian expression plasmids without an insert [108] or containing the A3H HapII coding sequence [27] were a generous gift from Viviana Simon (Mount Sinai School of Medicine, New York, NY) and had either no tag or an N-terminal Flag tag. A3H mutants were all

constructed in the pTR600 A3H-Flag vector using the QuikChange Lightning Site-Directed Mutagenesis Kit (Agilent Technologies, Santa Clara, CA) or the Tagmaster Site-Directed Mutagenesis Kit (GM Biosciences, Rockville, MD). For primer design, the on-line QuikChange Primer Design Program provided by the manufacturer or the design guidelines provided with the Tagmaster kit were used. Large-scale plasmid preparations were obtained using the HiSpeed Plasmid Maxi Prep kit (Qiagen, Inc.). The A3H sequence in each plasmid was verified by DNA sequencing performed by ACGT (Wheeling, IL).

Preparation of mammalian cell extracts

Propagation of 293T cells, transfection procedure, preparation of cell extracts, and determination of protein concentration were performed as detailed in Mitra et al. [42]. The expression levels of A3H were estimated by subjecting ~20 μg of total protein in the extract to Western blot analysis using the Western Breeze chemiluminescent Western blot kit (Life Technologies). The primary antibodies used for this analysis were anti-A3H or anti-tubulin (loading control).

Deaminase assay

Prior to performing the deaminase assay, the 293T cell extract (20 μg) was treated with RNase A (Qiagen, final concentration 1 μg/μl) in a 20-μl reaction volume and incubated at 37°C for 15 min, unless indicated otherwise. Details of the deaminase assays and polyacrylamide gel analysis are described in Mitra et al. [42]. A list of oligonucleotides used for the deaminase assays is given in Additional file 5: Table S1. Throughout the text, the dC residue that is deaminated is highlighted in bold (C). A 40-nt Alexa-Fluor 488-labeled ssDNA (JL913) containing the TT**C**A deaminase motif was used as the substrate, unless specified otherwise. To calculate the percent deaminase product, the product signal intensity for each lane was divided by total signal intensity and multiplied by 100. The data presented represent the average of two determinations from two independent transfections. Note that the FLAG tag did not interfere with deaminase activity, as untagged and tagged WT A3H showed similar levels of activity (Figure 4C).

HIV-1 infectivity assay

To assay the effect of expressing A3H WT or mutant proteins on HIV-1 infectivity, 293T cells were cotransfected with 1.0 μg of pNL4–3*vif* (–), which was kindly provided by Klaus Strebel (National Institute of Allergy and Infectious Diseases, National Institutes of Health, Bethesda, MD) and 1.0 or 0.1 μg of the pTR600 A3H HapII plasmid (WT or mutant) or pTR600 empty vector (control), using the FuGENE HD transfection agent (Promega, Madison, WI) as previously described [49]. Virus-containing supernatants were collected 48 h after transfection and filtered. The amount of CA protein (i.e., p24 antigen) in the supernatant was determined by ELISA assay (ZeptoMetrix, Buffalo, NY). TZM-bl indicator cells were infected with viral supernatant containing 10 ng of CA. Relative infectivity expressed as relative light units (RLU) was measured using the Bright-Glo luciferase assay system kit (Promega) and an ARVO MX luminescence counter (PerkinElmer, Waltham, MA). The data represent the results of three independent experiments.

ERT assay

The following plasmids were used: pTR600, empty vector; WT A3H HapII expressed as an N-terminal FLAG-tagged protein in pTR600 (pA3H WT); A3H E56A active site mutant expressed as an N-terminal FLAG-tagged protein in pTR600 (pA3H E56A); and pNL4-3*vif* (–).

Transfections were performed as described previously [109], except that TransIT-293 from Mirus Bio LLC (Madison, WI) was used, according to the manufacturer's instructions. Briefly, 100-mm cell culture dishes were seeded with 3×10^5 293T cells in Dulbecco's modified Eagle's Medium with 10% fetal bovine serum. Two days later, the cells were transfected in duplicate with 15 μg of pNL4-3*vif* (–) and 0, 1.5, or 5 μg of pA3H WT or pA3H E56A plasmid; the molar ratios of pNL4-3*vif* (–) to A3H plasmid were therefore 10:1 or 3:1, respectively. The pTR600 plasmid was the negative control and was also used to generate a constant level (5 μg) of transfected pTR600 DNA, with or without the A3H insert. Culture fluids were changed 24 h after transfection, then harvested after two consecutive 24-h periods, and passed through 0.22 μm filters. Samples from each culture were pooled and were treated sequentially with DNase I and subtilisin, as described [109,110].

ERT reactions were performed without Triton X-100 pretreatment and nucleic acids were isolated as detailed in Thomas et al. [109]. Real-time PCR for the detection of R-U5 and R-5'UTR was performed in duplicate as described previously [111]. The kinetics of DNA synthesis were plotted and the data were normalized relative to maximal R-U5 copies at 240 min for pNL4-3*vif* (–) in the absence of A3H cotransfected plasmid. Each data point was the result of two independent transfections, each measured in duplicate. Error bars represent the standard error of the mean.

Additional files

Additional file 1: Figure S1. Sequence alignment of residues in the Zn-binding (Z) domains of the seven A3 proteins (A to H). The Zn-coordinating (H and C) and active site (E) residues are highlighted in light blue. A3H residues that differ from highly conserved residues at the corresponding positions in the other A3 proteins are shown in lavender.

The residues in loop 7 are bracketed. The numbers at the end of each line represent the position in the full-length protein. The percent sequence identity of each Z domain relative to that of A3H (defined as 100%) is indicated. The sequence alignment was performed using Lasergene software (DNASTAR, Inc., Madison, WI).

Additional file 2: Figure S2. Superposition of the structures of the current A3H model and other A3 proteins in ribbon representation. The backbone traces are colored gray (A3H) and green (other A3 proteins). The Zn ions are shown in brown (A3H) and in coral (other A3 proteins). **(A)** A3H and A3G-CTD. **(B)** A3H and A3A. **(C)** A3H and A3C. **(D)** A3H and A3F-CTD.

Additional file 3: Figure S3. Electrostatic surface potential maps of A3H and other A3 proteins. **(A)** A3H. **(B)** A3G-CTD. **(C)** A3A. **(D)** A3C. **(E)** A3F-CTD. Regions with positive and negative electrostatic potentials are highlighted in blue and red, respectively.

Additional file 4: Figure S4. Comparison of antiviral activities of A3H and A3G WT and catalytic mutants. Virions produced from 293T cells transfected with HIV-1*vif*(–) (1 μg) and either 0.1 (gray bars) or 1 μg (black bars) of the indicated A3H or A3G WT or mutant plasmids. Infectivity was assayed as described in Methods. The catalytic mutants are E56A (A3H) and E259Q (A3G). A vector control (100% infectivity) was also included.

Additional file 5: Table S1. Oligonucleotides used for deaminase assays.

Abbreviations

A3: APOBEC3; ss: Single-stranded; HIV-1: Human immunodeficiency virus type 1; HTLV-1: Human T-lymphotropic virus type 1; HBV: Hepatitis B virus; CTD: C-terminal domain; NTD: N-terminal domain; WT: Wild type; ERT: Endogenous reverse transcription; CA: Capsid protein; RT: Reverse transcriptase.

Competing interests

The authors declare that they have no competing interests.

Authors' contributions

The study was conceived by MM and JGL. MM, DS, YM, GN, RJG, and YI performed experiments. MM, RJG, YI, and JGL analyzed the experimental data. JH built the structural model of A3H and MM and JH designed the mutants. I-JLB made the structural figures and I-JLB and JH interpreted the electrostatic surface potential maps. I-JLB, MM, and AMG interpreted the structure-related mutagenesis data. MM, I-JLB, YI, AMG, and JGL wrote the paper. All authors read and approved the final manuscript.

Acknowledgements

We thank Dr. Viviana Simon and Dr. Marcel Ooms for their generous gift of the WT A3H and empty pTR600 plasmids, Dr. Klaus Strebel for kindly providing the pNL4-3*vif*(–) plasmid used in the ERT assays, Drs. Simon, Ooms, and Tiyun Wu for valuable discussion, and the AIDS Research and Reference Reagent Program, Division of AIDS, NIAID, NIH for antisera and cells, as detailed in the text. J.H. acknowledges financial support by an International Outgoing Fellowship of the European Community program "Support for training and career development of researchers (Marie Curie)", under Contract No. PIOF-GA-2009-235902. This work was supported in part by the Intramural Research Program at the National Institutes of Health, Eunice Kennedy Shriver National Institute of Child Health and Human Development (MM, DS, GN, and JGL), National Institutes of Health grant P50GM82251 (JH, I-JLB, and AMG), and a grant-in-aid for Scientific Research from the Ministry of Education, Culture, Sports, Science, and Technology of Japan (YM and YI). This project has also been funded in whole or in part with federal funds from the National Cancer Institute, National Institutes of Health, under contract HHSN261200800001E with Leidos Biomedical Research, Inc. The content of this publication does not necessarily reflect the views or policies of the Department of Health and Human Services, nor does mention of trade names, commercial products, or organizations imply endorsement by the U.S. Government (RJG).

Author details

[1]Section on Viral Gene Regulation, Program in Genomics of Differentiation, Eunice Kennedy Shriver National Institute of Child Health and Human Development, National Institutes of Health, Bethesda, MD 20892-2780, USA. [2]Clinical Research Center, National Hospital Organization Nagoya Medical Center, Nagoya, Aichi 460-0001, Japan. [3]Department of Structural Biology, University of Pittsburgh Medical School, Pittsburgh, PA 15261, USA. [4]Pittsburgh Center for HIV Protein Interactions, University of Pittsburgh Medical School, Pittsburgh, PA 15261, USA. [5]AIDS and Cancer Virus Program, Leidos Biomedical Research, Inc., Frederick National Laboratory for Cancer Research, Frederick, MD 21702-1201, USA. [6]Department of Molecular, Cell and Developmental Biology, University of California, Los Angeles, CA 90095, USA. [7]Department of Structural Biology, CEITEC, Masaryk University, Kamenice 5, 625 00 Brno, Czech Republic.

Received: 14 October 2014 Accepted: 17 December 2014
Published online: 22 January 2015

References

1. Sheehy AM, Gaddis NC, Choi JD, Malim MH. Isolation of a human gene that inhibits HIV-1 infection and is suppressed by the viral Vif protein. Nature. 2002;418:646–50.
2. Lecossier D, Bouchonnet F, Clavel F, Hance AJ. Hypermutation of HIV-1 DNA in the absence of the Vif protein. Science. 2003;300:1112.
3. Zhang H, Yang B, Pomerantz RJ, Zhang C, Arunachalam SC, Gao L. The cytidine deaminase CEM15 induces hypermutation in newly synthesized HIV-1 DNA. Nature. 2003;424:94–8.
4. Suspène R, Sommer P, Henry M, Ferris S, Guétard D, Pochet S, et al. APOBEC3G is a single-stranded DNA cytidine deaminase and functions independently of HIV reverse transcriptase. Nucleic Acids Res. 2004;32:2421–9.
5. Yu Q, König R, Pillai S, Chiles K, Kearney M, Palmer S, et al. Single-strand specificity of APOBEC3G accounts for minus-strand deamination of the HIV genome. Nat Struct Mol Biol. 2004;11:435–42.
6. Harris RS, Liddament MT. Retroviral restriction by APOBEC proteins. Nat Rev Immunol. 2004;4:868–77.
7. Chiu YL, Greene WC. The APOBEC3 cytidine deaminases: an innate defensive network opposing exogenous retroviruses and endogenous retroelements. Annu Rev Immunol. 2008;26:317–53.
8. Goila-Gaur R, Strebel K. HIV-1 Vif, APOBEC, and intrinsic immunity. Retrovirology. 2008;5:51.
9. Malim MH. APOBEC proteins and intrinsic resistance to HIV-1 infection. Philos Trans R Soc Lond B Biol Sci. 2009;364:675–87.
10. Imahashi M, Nakashima M, Iwatani Y. Antiviral mechanism and biochemical basis of the human APOBEC3 family. Front Microbiol. 2012;3:250.
11. Duggal NK, Fu W, Akey JM, Emerman M. Identification and antiviral activity of common polymorphisms in the APOBEC3 locus in human populations. Virology. 2013;443:329–37.
12. Desimmie BA, Delviks-Frankenberrry KA, Burdick RC, Qi D, Izumi T, Pathak VK. Multiple APOBEC3 restriction factors for HIV-1 and one Vif to rule them all. J Mol Biol. 2014;426:1220–45.
13. Feng Y, Baig TT, Love RP, Chelico L. Suppression of APOBEC3-mediated restriction of HIV-1 by Vif. Front Microbiol. 2014;5:450.
14. Sasada A, Takaori-Kondo A, Shirakawa K, Kobayashi M, Abudu A, Hishizawa M, et al. APOBEC3G targets human T-cell leukemia virus type 1. Retrovirology. 2005;2:32.
15. Ooms M, Krikoni A, Kress AK, Simon V, Münk C. APOBEC3A, APOBEC3B, and APOBEC3H haplotype 2 restrict human T-lymphotropic virus type 1. J Virol. 2012;86:6097–108.
16. Turelli P, Mangeat B, Jost S, Vianin S, Trono D. Inhibition of hepatitis B virus replication by APOBEC3G. Science. 2004;303:1829.
17. Köck J, Blum HE. Hypermutation of hepatitis B virus genomes by APOBEC3G, APOBEC3C and APOBEC3H. J Gen Virol. 2008;89:1184–91.
18. Koito A, Ikeda T. Intrinsic immunity against retrotransposons by APOBEC cytidine deaminases. Front Microbiol. 2013;4:28.
19. Jarmuz A, Chester A, Bayliss J, Gisbourne J, Dunham I, Scott J, et al. An anthropoid-specific locus of orphan C to U RNA-editing enzymes on chromosome 22. Genomics. 2002;79:285–96.
20. Holmes RK, Malim MH, Bishop KN. APOBEC-mediated viral restriction: not simply editing? Trends Biochem Sci. 2007;32:118–28.
21. Bransteitter R, Prochnow C, Chen XS. The current structural and functional understanding of APOBEC deaminases. Cell Mol Life Sci. 2009;66:3137–47.

22. Betts L, Xiang S, Short SA, Wolfenden R, Carter Jr CW. Cytidine deaminase. The 2.3 Å crystal structure of an enzyme: transition-state analog complex. J Mol Biol. 1994;235:635–56.
23. LaRue RS, Jónsson SR, Silverstein KAT, Lajoie M, Bertrand D, El-Mabrouk N, et al. The artiodactyl APOBEC3 innate immune repertoire shows evidence for a multi-functional domain organization that existed in the ancestor of placental mammals. BMC Mol Biol. 2008;9:104.
24. LaRue RS, Andrésdóttir V, Blanchard Y, Conticello SG, Derse D, Emerman M, et al. Guidelines for naming nonprimate APOBEC3 genes and proteins. J Virol. 2009;83:494–7.
25. OhAinle M, Kerns JA, Malik HS, Emerman M. Adaptive evolution and antiviral activity of the conserved mammalian cytidine deaminase *APOBEC3H*. J Virol. 2006;80:3853–62.
26. OhAinle M, Kerns JA, Li MMH, Malik HS, Emerman M. Antiretroelement activity of APOBEC3H was lost twice in recent human evolution. Cell Host Microbe. 2008;4:249–59.
27. Harari A, Ooms M, Mulder LCF, Simon V. Polymorphisms and splice variants influence the antiretroviral activity of human APOBEC3H. J Virol. 2009;83:295–303.
28. Ooms M, Majdak S, Seibert CW, Harari A, Simon V. The localization of APOBEC3H variants in HIV-1 virions determines their antiviral activity. J Virol. 2010;84:7961–9.
29. Wang X, Abudu A, SungMo S, Dang Y, Venta PJ, Zheng Y-H. Analysis of human APOBEC3H haplotypes and anti-human immunodeficiency virus type 1 activity. J Virol. 2011;85:3142–52.
30. Li MMH, Wu LI, Emerman M. The range of human APOBEC3H sensitivity to lentiviral Vif proteins. J Virol. 2010;84:88–95.
31. Zhen A, Wang T, Zhao K, Xiong Y, Yu X-F. A single amino acid difference in human APOBEC3H variants determines HIV-1 Vif sensitivity. J Virol. 2010;84:1902–11.
32. Ooms M, Brayton B, Letko M, Maio SM, Pilcher CD, Hecht FM, et al. HIV-1 Vif adaptation to human APOBEC3H haplotypes. Cell Host Microbe. 2013;14:411–21.
33. Binka M, Ooms M, Steward M, Simon V. The activity spectrum of Vif from multiple HIV-1 subtypes against APOBEC3G, APOBEC3F, and APOBEC3H. J Virol. 2012;86:49–59.
34. Ooms M, Letko M, Binka M, Simon V. The resistance of human APOBEC3H to HIV-1 NL4-3 molecular clone is determined by a single amino acid in Vif. PLoS One. 2013;8:e57744.
35. Chen H, Lilley CE, Yu Q, Lee DV, Chou J, Narvaiza I, et al. APOBEC3A is a potent inhibitor of adeno-associated virus and retrotransposons. Curr Biol. 2006;16:480–5.
36. Aguiar RS, Lovsin N, Tanuri A, Peterlin BM. Vpr.A3A chimera inhibits HIV replication. J Biol Chem. 2008;283:2518–25.
37. Stenglein MD, Burns MB, Li M, Lengyel J, Harris RS. APOBEC3 proteins mediate the clearance of foreign DNA from human cells. Nat Struct Mol Biol. 2010;17:222–9.
38. Bulliard Y, Narvaiza I, Bertero A, Peddi S, Röhrig UF, Ortiz M, et al. Structure-function analyses point to a polynucleotide-accommodating groove essential for APOBEC3A restriction activities. J Virol. 2011;85:1765–76.
39. Love RP, Xu H, Chelico L. Biochemical analysis of hypermutation by the deoxycytidine deaminase APOBEC3A. J Biol Chem. 2012;287:30812–22.
40. Shinohara M, Io K, Shindo K, Matsui M, Sakamoto T, Tada K, et al. APOBEC3B can impair genomic stability by inducing base substitutions in genomic DNA in human cells. Sci Rep. 2012;2:806.
41. Byeon I-JL, Ahn J, Mitra M, Byeon C-H, Hercík K, Hritz J, et al. NMR structure of human restriction factor APOBEC3A reveals substrate binding and enzyme specificity. Nat Commun. 2013;4:1890.
42. Mitra M, Hercík K, Byeon I-JL, Ahn J, Hill S, Hinchee-Rodriguez K, et al. Structural determinants of human APOBEC3A enzymatic and nucleic acid binding properties. Nucleic Acids Res. 2014;42:1095–110.
43. Holden LG, Prochnow C, Chang YP, Bransteitter R, Chelico L, Sen U, et al. Crystal structure of the anti-viral APOBEC3G catalytic domain and functional implications. Nature. 2008;456:121–4.
44. Carpenter MA, Rajagurubandara E, Wijesinghe P, Bhagwat AS. Determinants of sequence-specificity within human AID and APOBEC3G. DNA Repair. 2010;9:579–87.
45. Kohli RM, Maul RW, Guminski AF, McClure RL, Gajula KS, Saribasak H, et al. Local sequence targeting in the AID/APOBEC family differentially impacts retroviral restriction and antibody diversification. J Biol Chem. 2010;285:40956–64.
46. Rathore A, Carpenter MA, Demir Ö, Ikeda T, Li M, Shaban NM, et al. The local dinucleotide preference of APOBEC3G can be altered from 5'-CC to 5'-TC by a single amino acid substitution. J Mol Biol. 2013;425:4442–54.
47. Aydin H, Taylor MW, Lee JE. Structure-guided analysis of the human APOBEC3-HIV restrictome. Structure. 2014;22:668–84.
48. Kim E-Y, Lorenzo-Redondo R, Little SJ, Chung Y-S, Phalora PK, Maljkovic Berry I, et al. Human APOBEC3 induced mutation of human immunodeficiency virus type-1 contributes to adaptation and evolution in natural infection. PLoS Pathog. 2014;10:e1004281.
49. Kitamura S, Ode H, Nakashima M, Imahashi M, Naganawa Y, Kurosawa T, et al. The APOBEC3C crystal structure and the interface for HIV-1 Vif binding. Nat Struct Mol Biol. 2012;19:1005–10.
50. Chen KM, Harjes E, Gross PJ, Fahmy A, Lu Y, Shindo K, et al. Structure of the DNA deaminase domain of the HIV-1 restriction factor APOBEC3G. Nature. 2008;452:116–9.
51. Furukawa A, Nagata T, Matsugami A, Habu Y, Sugiyama R, Hayashi F, et al. Structure, interaction and real-time monitoring of the enzymatic reaction of wild-type APOBEC3G. EMBO J. 2009;28:440–51.
52. Harjes E, Gross PJ, Chen K-M, Lu Y, Shindo K, Nowarski R, et al. An extended structure of the APOBEC3G catalytic domain suggests a unique holoenzyme model. J Mol Biol. 2009;389:819–32.
53. Shandilya SMD, Nalam MNL, Nalivaika EA, Gross PJ, Valesano JC, Shindo K, et al. Crystal structure of the APOBEC3G catalytic domain reveals potential oligomerization interfaces. Structure. 2010;18:28–38.
54. Bohn M-F, Shandilya SMD, Albin JS, Kouno T, Anderson BD, McDougle RM, et al. Crystal structure of the DNA cytosine deaminase APOBEC3F: the catalytically active and HIV-1 Vif-binding domain. Structure. 2013;21:1042–50.
55. Siu KK, Sultana A, Azimi FC, Lee JE. Structural determinants of HIV-1 Vif susceptibility and DNA binding in APOBEC3F. Nat Commun. 2013;4:2593.
56. Šali A, Blundell TL. Comparative protein modelling by satisfaction of spatial restraints. J Mol Biol. 1993;234:779–815.
57. Zhen A, Du J, Zhou X, Xiong Y, Yu X-F. Reduced APOBEC3H variant anti-viral activities are associated with altered RNA binding activities. PLoS One. 2012;7:e38771.
58. Haché G, Liddament MT, Harris RS. The retroviral hypermutation specificity of APOBEC3F and APOBEC3G is governed by the C-terminal DNA cytosine deaminase domain. J Biol Chem. 2005;280:10920–4.
59. Langlois M-A, Beale RCL, Conticello SG, Neuberger MS. Mutational comparison of the single-domained APOBEC3C and double-domained APOBEC3F/G anti-retroviral cytidine deaminases provides insight into their DNA target site specificities. Nucleic Acids Res. 2005;33:1913–23.
60. Navarro F, Bollman B, Chen H, König R, Yu Q, Chiles K, et al. Complementary function of the two catalytic domains of APOBEC3G. Virology. 2005;333:374–86.
61. Iwatani Y, Takeuchi H, Strebel K, Levin JG. Biochemical activities of highly purified, catalytically active human APOBEC3G: correlation with antiviral effect. J Virol. 2006;80:5992–6002.
62. Hultquist JF, Lengyel JA, Refsland EW, LaRue RS, Lackey L, Brown WL, et al. Human and rhesus APOBEC3D, APOBEC3F, APOBEC3G, and APOBEC3H demonstrate a conserved capacity to restrict Vif-deficient HIV-1. J Virol. 2011;85:11220–34.
63. McDougall WM, Smith HC. Direct evidence that RNA inhibits APOBEC3G ssDNA cytidine deaminase activity. Biochem Biophys Res Commun. 2011;412:612–7.
64. Huthoff H, Autore F, Gallois-Montbrun S, Fraternali F, Malim MH. RNA-dependent oligomerization of APOBEC3G is required for restriction of HIV-1. PLoS Pathog. 2009;5:e1000330.
65. Newman ENC, Holmes RK, Craig HM, Klein KC, Lingappa JR, Malim MH, et al. Antiviral function of APOBEC3G can be dissociated from cytidine deaminase activity. Curr Biol. 2005;15:166–70.
66. Bishop KN, Holmes RK, Malim MH. Antiviral potency of APOBEC proteins does not correlate with cytidine deamination. J Virol. 2006;80:8450–8.
67. Guo F, Cen S, Niu M, Saadatmand J, Kleiman L. Inhibition of $tRNA_3^{Lys}$-primed reverse transcription by human APOBEC3G during human immunodeficiency virus type 1 replication. J Virol. 2006;80:11710–22.
68. Holmes RK, Koning FA, Bishop KN, Malim MH. APOBEC3F can inhibit the accumulation of HIV-1 reverse transcription products in the absence of hypermutation. Comparisons with APOBEC3G. J Biol Chem. 2007;282:2587–95.
69. Iwatani Y, Chan DSB, Wang F, Maynard KS, Sugiura W, Gronenborn AM, et al. Deaminase-independent inhibition of HIV-1 reverse transcription by APOBEC3G. Nucleic Acids Res. 2007;35:7096–108.

70. Li X-Y, Guo F, Zhang L, Kleiman L, Cen S. APOBEC3G inhibits DNA strand transfer during HIV-1 reverse transcription. J Biol Chem. 2007;282:32065–74.
71. Luo K, Wang T, Liu B, Tian C, Xiao Z, Kappes J, et al. Cytidine deaminases APOBEC3G and APOBEC3F interact with human immunodeficiency virus type 1 integrase and inhibit proviral DNA formation. J Virol. 2007;81:7238–48.
72. Mbisa JL, Barr R, Thomas JA, Vandegraaff N, Dorweiler IJ, Svarovskaia ES, et al. Human immunodeficiency virus type 1 cDNAs produced in the presence of APOBEC3G exhibit defects in plus-strand DNA transfer and integration. J Virol. 2007;81:7099–110.
73. Bishop KN, Verma M, Kim E-Y, Wolinsky SM, Malim MH. APOBEC3G inhibits elongation of HIV-1 reverse transcripts. PLoS Pathog. 2008;4:e1000231.
74. Levin JG, Mitra M, Mascarenhas A, Musier-Forsyth K. Role of HIV-1 nucleocapsid protein in HIV-1 reverse transcription. RNA Biol. 2010;7:754–74.
75. Wang X, Ao Z, Chen L, Kobinger G, Peng J, Yao X. The cellular antiviral protein APOBEC3G interacts with HIV-1 reverse transcriptase and inhibits its function during viral replication. J Virol. 2012;86:3777–86.
76. Adolph MB, Webb J, Chelico L. Retroviral restriction factor APOBEC3G delays the initiation of DNA synthesis by HIV-1 reverse transcriptase. PLoS One. 2013;8:e64196.
77. Bélanger K, Savoie M, Rosales Gerpe MC, Couture J-F, Langlois M-A. Binding of RNA by APOBEC3G controls deamination-independent restriction of retroviruses. Nucleic Acids Res. 2013;41:7438–52.
78. Gillick K, Pollpeter D, Phalora P, Kim E-Y, Wolinsky SM, Malim MH. Suppression of HIV-1 infection by APOBEC3 proteins in primary human $CD4^+$ T cells is associated with inhibition of processive reverse transcription as well as excessive cytidine deamination. J Virol. 2013;87:1508–17.
79. Chaurasiya KR, McCauley MJ, Wang W, Qualley DF, Wu T, Kitamura S, et al. Oligomerization transforms human APOBEC3G from an efficient enzyme to a slowly dissociating nucleic acid-binding protein. Nat Chem. 2014;6:28–33.
80. Dang Y, Siew LM, Wang X, Han Y, Lampen R, Zheng YH. Human cytidine deaminase APOBEC3H restricts HIV-1 replication. J Biol Chem. 2008;283:11606–14.
81. Shandilya SMD, Bohn M-F, Schiffer CA. A computational analysis of the structural determinants of APOBEC3's catalytic activity and vulnerability to HIV-1 Vif. Virology. 2014;471–473:105–16.
82. Chiu Y-L, Witkowska HE, Hall SC, Santiago M, Soros VB, Esnault C, et al. High-molecular-mass APOBEC3G complexes restrict Alu retrotransposition. Proc Natl Acad Sci U S A. 2006;103:15588–93.
83. Kozak SL, Marin M, Rose KM, Bystrom C, Kabat D. The anti-HIV-1 editing enzyme APOBEC3G binds HIV-1 RNA and messenger RNAs that shuttle between polysomes and stress granules. J Biol Chem. 2006;281:29105–19.
84. Gallois-Montbrun S, Kramer B, Swanson CM, Byers H, Lynham S, Ward M, et al. Antiviral protein APOBEC3G localizes to ribonucleoprotein complexes found in P bodies and stress granules. J Virol. 2007;81:2165–78.
85. Chelico L, Sacho EJ, Erie DA, Goodman MF. A model for oligomeric regulation of APOBEC3G cytosine deaminase-dependent restriction of HIV. J Biol Chem. 2008;283:13780–91.
86. Gallois-Montbrun S, Holmes RK, Swanson CM, Fernández-Ocaña M, Byers HL, Ward MA, et al. Comparison of cellular ribonucleoprotein complexes associated with the APOBEC3F and APOBEC3G antiviral proteins. J Virol. 2008;82:5636–42.
87. Friew YN, Boyko V, Hu W-S, Pathak VK. Intracellular interactions between APOBEC3G, RNA, and HIV-1 Gag: APOBEC3G multimerization is dependent on its association with RNA. Retrovirology. 2009;6:56.
88. Salter JD, Krucinska J, Raina J, Smith HC, Wedekind JE. A hydrodynamic analysis of APOBEC3G reveals a monomer-dimer-tetramer self-association that has implications for anti-HIV function. Biochemistry. 2009;48:10685–7.
89. Chelico L, Prochnow C, Erie DA, Chen XS, Goodman MF. Structural model for deoxycytidine deamination mechanisms of the HIV-1 inactivation enzyme APOBEC3G. J Biol Chem. 2010;285:16195–205.
90. McDougall WM, Okany C, Smith HC. Deaminase activity on single-stranded DNA (ssDNA) occurs *in vitro* when APOBEC3G cytidine deaminase forms homotetramers and higher-order complexes. J Biol Chem. 2011;286:30655–61.
91. Shlyakhtenko LS, Lushnikov AY, Li M, Lackey L, Harris RS, Lyubchenko YL. Atomic force microscopy studies provide direct evidence for dimerization of the HIV restriction factor APOBEC3G. J Biol Chem. 2011;286:3387–95.
92. Li J, Chen Y, Li M, Carpenter MA, McDougle RM, Luengas EM, et al. APOBEC3 multimerization correlates with HIV-1 packaging and restriction activity in living cells. J Mol Biol. 2014;426:1296–307.
93. Baig TT, Feng Y, Chelico L. Determinants of efficient degradation of APOBEC3 restriction factors by HIV-1 Vif. J Virol. 2014;88:14380–95.
94. Tan L, Sarkis PTN, Wang T, Tian C, Yu X-F. Sole copy of Z2-type human cytidine deaminase APOBEC3H has inhibitory activity against retrotransposons and HIV-1. FASEB J. 2009;23:279–87.
95. Goila-Gaur R, Khan MA, Miyagi E, Kao S, Strebel K. Targeting APOBEC3A to the viral nucleoprotein complex confers antiviral activity. Retrovirology. 2007;4:61.
96. Song C, Sutton L, Johnson ME, D'Aquila RT, Donahue JP. Signals in APOBEC3F N-terminal and C-terminal deaminase domains each contribute to encapsidation in HIV-1 virions and are both required for HIV-1 restriction. J Biol Chem. 2012;287:16965–74.
97. Bennett RP, Diner E, Sowden MP, Lees JA, Wedekind JE, Smith HC. APOBEC-1 and AID are nucleo-cytoplasmic trafficking proteins but APOBEC3G cannot traffic. Biochem Biophys Res Commun. 2006;350:214–9.
98. Wichroski MJ, Robb GB, Rana TM. Human retroviral host restriction factors APOBEC3G and APOBEC3F localize to mRNA processing bodies. PLoS Pathog. 2006;2:e41.
99. Bennett RP, Presnyak V, Wedekind JE, Smith HC. Nuclear exclusion of the HIV-1 host defense factor APOBEC3G requires a novel cytoplasmic retention signal and is not dependent on RNA binding. J Biol Chem. 2008;283:7320–7.
100. Li MMH, Emerman M. Polymorphism in human APOBEC3H affects a phenotype dominant for subcellular localization and antiviral activity. J Virol. 2011;85:8197–207.
101. Chelico L, Pham P, Calabrese P, Goodman MF. APOBEC3G DNA deaminase acts processively 3' → 5' on single-stranded DNA. Nat Struct Mol Biol. 2006;13:392–9.
102. Platt EJ, Wehrly K, Kuhmann SE, Chesebro B, Kabat D. Effects of CCR5 and CD4 cell surface concentrations on infections by macrophagetropic isolates of human immunodeficiency virus type 1. J Virol. 1998;72:2855–64.
103. Derdeyn CA, Decker JM, Sfakianos JN, Wu X, O'Brien WA, Ratner L, et al. Sensitivity of human immunodeficiency virus type 1 to the fusion inhibitor T-20 is modulated by coreceptor specificity defined by the V3 loop of gp120. J Virol. 2000;74:8358–67.
104. Wei X, Decker JM, Liu H, Zhang Z, Arani RB, Kilby JM, et al. Emergence of resistant human immunodeficiency virus type 1 in patients receiving fusion inhibitor (T-20) monotherapy. Antimicrob Agents Chemother. 2002;46:1896–905.
105. Wang J, Wolf RM, Caldwell JW, Kollman PA, Case DA. Development and testing of a general amber force field. J Comput Chem. 2004;25:1157–74.
106. Dolinsky TJ, Czodrowski P, Li H, Nielsen JE, Jensen JH, Klebe G, et al. PDB2PQR: expanding and upgrading automated preparation of biomolecular structures for molecular simulations. Nucleic Acids Res. 2007;35:W522–5.
107. Koradi R, Billeter M, Wüthrich K. MOLMOL: a program for display and analysis of macromolecular structures. J Mol Graph. 1996;14:51–5.
108. Green TD, Newton BR, Rota PA, Xu Y, Robinson HL, Ross TM. C3d enhancement of neutralizing antibodies to measles hemagglutinin. Vaccine. 2001;20:242–8.
109. Thomas JA, Shatzer TL, Gorelick RJ. Blocking premature reverse transcription fails to rescue the HIV-1 nucleocapsid-mutant replication defect. Retrovirology. 2011;8:46.
110. Ott DE, Coren LV, Johnson DG, Sowder II RC, Arthur LO, Henderson LE. Analysis and localization of cyclophilin A found in the virions of human immunodeficiency virus type 1 MN strain. AIDS Res Hum Retroviruses. 1995;11:1003–6.
111. Thomas JA, Gagliardi TD, Alvord WG, Lubomirski M, Bosche WJ, Gorelick RJ. Human immunodeficiency virus type 1 nucleocapsid zinc-finger mutations cause defects in reverse transcription and integration. Virology. 2006;353:41–51.

The FASEB Journal • Research Communication

Structural basis of clade-specific HIV-1 neutralization by humanized anti-V3 monoclonal antibody KD-247

Karen A. Kirby,[*,†,1] Yee Tsuey Ong,[*,†,1] Atsuko Hachiya,[*,†] Thomas G. Laughlin,[*,†] Leslie A. Chiang,[*,†] Yun Pan,[*,†] Jennifer L. Moran,[*,†] Bruno Marchand,[*,†] Kamalendra Singh,[*,†] Fabio Gallazzi,[‡] Thomas P. Quinn,[§] Kazuhisa Yoshimura,[¶] Toshio Murakami,[‖] Shuzo Matsushita,[#] and Stefan G. Sarafianos[*,†,§,2]

[*]Christopher S. Bond Life Sciences Center, [†]Department of Molecular Microbiology and Immunology, School of Medicine, [‡]Structural Biology Core, and [§]Department of Biochemistry, University of Missouri, Columbia, Missouri, USA; [¶]AIDS Research Center, National Institute of Infectious Diseases, Tokyo, Japan; [‖]The Chemo-Sero-Therapeutic Research Institute (Kaketsuken), Kyokushi, Kikuchi, Kumamoto, Japan; and [#]Division of Clinical Retrovirology and Infectious Diseases, Center for AIDS Research, Kumamoto University, Kumamoto, Japan

ABSTRACT **Humanized monoclonal antibody KD-247 targets the Gly^{312}-Pro^{313}-Gly^{314}-Arg^{315} arch of the third hypervariable (V3) loop of the HIV-1 surface glycoprotein. It potently neutralizes many HIV-1 clade B isolates, but not of other clades. To understand the molecular basis of this specificity, we solved a high-resolution (1.55 Å) crystal structure of the KD-247 antigen binding fragment and examined the potential interactions with various V3 loop targets. Unlike most antibodies, KD-247 appears to interact with its target primarily through light chain residues. Several of these interactions involve Arg^{315} of the V3 loop. To evaluate the role of light chain residues in the recognition of the V3 loop, we generated 20 variants of KD-247 single-chain variable fragments with mutations in the antigen-binding site. Purified proteins were assessed for V3 loop binding using AlphaScreen technology and for HIV-1 neutralization. Our data revealed that recognition of the clade-specificity defining residue Arg^{315} of the V3 loop is based on a network of interactions that involve Tyr^{L32}, Tyr^{L92}, and Asn^{L27d} that directly interact with Arg^{315}, thus elucidating the molecular interactions of KD-247 with its V3 loop target.—Kirby, K. A., Ong, Y. T., Hachiya, A., Laughlin, T. G., Chiang, L. A., Pan, Y., Moran, J. L., Marchand, B., Singh, K., Gallazzi, F., Quinn, T. P., Yoshimura, K., Murakami, T., Matsushita, S., Sarafianos, S. G. Structural basis of clade-specific HIV-1 neutralization by humanized anti-V3 monoclonal antibody KD-247. *FASEB J.* 29, 70–80 (2015). www.fasebj.org**

Key Words: crystal structure · entry · HIV · single-chain variable fragment

ALTHOUGH THE AVAILABILITY of highly active antiretroviral therapy (HAART) has significantly reduced the rate of HIV-1-related deaths (1), the development of a vaccine against multiple HIV-1 clades remains a challenge. The extensive glycosylation of the envelope glycoprotein (Env) (2) and the shedding of Env from the virus surface (3) are two of several mechanisms by which HIV-1 escapes the host immune system. Although most of the neutralizing antibodies elicited after HIV-1 infection are clade specific (4), some are broadly neutralizing, including b12 (5), 2G12 (6), 4E10 (7), 2F5 (8), PG9 and PG16 (9), VRC01 and VRC02 (10), PGT121-145 (11), NIH45-46 (12), and 10E8 (13).

HIV-1 Env comprises the noncovalently associated gp120 and gp41, which are proteolytic cleavage products of the gp160 precursor (14). The third hypervariable (V3) loop of gp120 that interacts with the CCR5 or CXCR4 coreceptor during HIV-1 entry (15) is one of the most immunodominant regions of HIV-1 (16–18). V3 loops of different HIV-1 strains and clades are highly variable in sequence and structural conformation (19). Anti-V3 antibodies elicited from animal immunization studies are generally clade-specific and show little or no cross-reactivity (19). Nevertheless, several anti-V3 antibodies, such as 447-52D, 2219, F425-B4e8, 2557, and 3074, have been reported to show cross-reactivity against a panel of HIV-1 isolates from various clades (20–25). The recent discovery of broadly neutralizing V3-targeting PGT121 and PGT128 antibodies continues to shed light on V3 loop immunogen design (26).

KD-247 is a humanized version of the C25 murine monoclonal antibody (mAb), which was isolated from the sequential immunization of mice with clade B HIV-1 V3 loop peptides (27). KD-247 can neutralize a broad

Abbreviations: CD, circular dichroism; CDR, complementarity determining region; Env, envelope glycoprotein; Fab, antigen-binding fragment; GPGR, Gly^{312}-Pro^{313}-Gly^{314}-Arg^{315}; mAb, monoclonal antibody; scFv, single-chain variable fragment; V3 loop, third hypervariable loop

[1] These authors contributed equally to this work.

[2] Correspondence: 471d Christopher S. Bond Life Sciences Center, 1201 Rollins St., Columbia, MO 65211, USA. E-mail: sarafianoss@missouri.edu

doi: 10.1096/fj.14-252262

This article includes supplemental data. Please visit *http://www.fasebj.org* to obtain this information.

spectrum of CCR5- and CXCR4-tropic viruses and HIV-1 quasi-species from patient plasma and peripheral blood mononuclear cells (27, 28). Passive transfer of KD-247 in simian/human immunodeficiency virus–infected monkeys protected the animals against $CD4^+$ T cell loss and increase of virus load (29, 30). This suggests that KD-247 can serve as a potential immunotherapy component in treating HIV-1-infected patients. Therefore, a structural understanding of the KD-247–V3 interactions should help us design strategies for expanding the clade specificity of this antibody.

The minimum V3 sequence required for KD-247 binding was mapped to Ile^{309}-Gly^{312}-Pro^{313}-Gly^{314}-Arg^{315} (IGPGR) at the V3 arch, and Arg^{315} is crucial for the interaction with KD-247 (27). We hypothesized that the interactions of KD-247 with residue 315 of the V3 loop strongly affect the clade specificity of KD-247, which can efficiently neutralize clade B viruses with Arg^{315} at the V3 arch, but not viruses from other clades that have a Gln^{315} (*e.g.*, Gly^{312}-Pro^{313}-Gly^{314}-Gln^{315} in most non–clade B viruses).

To understand the molecular basis of KD-247 clade specificity, we have solved the crystal structure of its unliganded antigen binding fragment (Fab) and used it in molecular modeling studies with V3 peptides to obtain insights into possible binding interactions between the Fab and the target V3 loop. The proposed interactions were validated by site-specific mutagenesis of single-chain variable fragment (scFv) KD-247 variants, peptide binding assays, and cell-based HIV-1 neutralization assays.

MATERIALS AND METHODS

Fab production and purification

KD-247 was obtained from the Chemo-Sero-Therapeutic Research Institute (27). Fab was prepared by digesting KD-247 (34°C, 7 h) with 0.2 mg of papain agarose (Sigma-Aldrich, St. Louis, MO, USA) per milligram of antibody at 2 mg/ml in sodium acetate pH 5.5, 50 mM L-cysteine and 1 mM EDTA. The reaction was stopped by removing the papain agarose using a 0.22 μm filter. Digested Fab was purified with a HiTrap SP HP 5 ml column (GE Healthcare, Piscataway, NJ, USA) using sodium acetate pH 5.5 as the binding buffer and sodium acetate pH 5.5, 1 M NaCl, as the elution buffer.

Crystallization and data collection

KD-247 Fab crystals were grown in sitting drop trays. Drops containing 1 μl Fab (10 mg/ml) and 1 μl well solution were allowed to equilibrate with 0.5 ml 1.9 M ammonium sulfate/0.05 M sodium acetate pH 4.4 at 21°C. Octahedral-shaped crystals appeared after 3 d and cryoprotected with 20% glycerol. Data were processed to 1.55 Å using d*TREK (31), and indexed in $P2_12_12_1$ (a = 61.1 Å, b = 69.2 Å, and c = 111.8 Å) with one Fab per asymmetric unit. The Matthews coefficient (32) was 2.5 $Å^3$/Da (solvent content ~51%).

Structure determination and refinement

The structure was determined by molecular replacement MOLREP (33). The Fab variable and constant domains of 1T3F from the Protein Data Bank (PDB) were treated as separate search models. After initial rigid-body and restrained refinement in Phenix (34), R_{work} dropped to 0.3377, with an R_{free} of 0.3560. Simulated annealing was used to remove model bias. An initial model was built using ARP/wARP (35) with refinement using Refmac (36). Several cycles of model building and refinement were carried out using Coot (37) and Phenix (**Table 1**). Final atomic coordinates and structure factors have been deposited (PDB ID: 3NTC).

Superposition analysis

The coordinates of several Fab–V3 peptide complexes were downloaded from the PDB: 1ACY, 1AI1, 1F58, 1GGI, 1NAK, 1Q1J, 2B0S, 2QSC, and 3MLW. These complexes were chosen specifically because all have V3 peptides based on the HIV-1_{MN} sequence, which is efficiently neutralized by KD-247. The Fab portions were aligned with the KD-247 Fab in Coot using the light chain for alignment. Upon each alignment, the position of the V3 peptide with respect to the KD-247 complementarity determining region (CDR) was visually inspected. The V3 peptide that fit best in the KD-247 binding pocket

TABLE 1. *Data collection and refinement statistics*

Data collection	Value
Wavelength (Å)	1.07
Resolution (Å)	1.55 (1.61–1.55)[a]
Space group	$P2_12_12_1$
Cell dimensions	
a (Å)	61.1
b (Å)	69.2
c (Å)	111.8
Observed reflections	448,730
Unique reflections	68,709
Redundancy	6.5 (4.4)
Completeness (%)	99.0 (92.0)
R_{sym}[b]	0.068 (0.595)
Avg I/σ	10.2 (1.6)
Refinement statistics for all reflections >0.0 σ F	
Resolution (Å)	19.75–1.55
No. of reflections (working)	68,481
No. of reflections (test)	2,748
R_{work}[c]	0.1901
R_{free}[d]	0.2099
No. of Fab atoms	3365
No. of water molecules	575
No. of solvent molecules	30
Overall B value ($Å^2$)	
Fab	26.28
Solvents	39.54
Wilson B value ($Å^2$)	24.16
Ramachandran plot (%)[e]	
Favored	98.2
Allowed	1.8
Disallowed	0.0
RMSD bond length (Å)	0.004
RMSD angle (°)	0.992

[a]Values in parentheses are for the outer resolution shell. [b]$R_{sym} = \Sigma_{hkl} |I - < I >| / \Sigma_{hkl} |I|$. [c]$R_{cryst} = \Sigma_{hkl} |F_{obs} - F_{calc}| / \Sigma_{hkl} |F_{obs}|$. [d]$R_{free} = R_{cryst}$, except 4% of the data excluded from the refinement. [e]Evaluated by MolProbity (48).

was from 2QSC (RP142 V3). The V3 peptide from the aligned 2QSC coordinates was removed and loaded with KD-247 into SYBYL (7.3.5; Tripos, St. Louis, MO, USA) and taken through a slight minimization procedure to reduce minor steric interactions.

Modeling of G314E and R315K KD-247-resistant V3 peptides with KD-247

Models of the G314E and R315K V3 peptides were generated by performing a simple mutation of the aligned and minimized RP142 peptide used in the superposition analysis at the 314 and 315 positions. All possible rotamers of Glu^{314} and Lys^{315} demonstrated steric clashes with KD-247 CDR residues.

Preparation of KD-247 scFv variants

Single amino acid substitutions of Asn^{L27d}, Tyr^{L32}, and Tyr^{L92} in the background pET28a3c-KD247 scFv (38) were generated by site-directed mutagenesis and verified by DNA sequencing. scFv variants were expressed in BL21(DE3) *Escherichia coli* and purified as previously described (38). scFv in the inclusion bodies was denatured and refolded before purification on HisTrap and HiPrep 26/60 Sephacryl S200 HR columns (GE Healthcare, Piscataway, NJ, USA). The secondary structure of the refolded scFv was examined using far-UV circular dichroism (CD) spectroscopy as previously described (38). Data were collected on a J-815 CD Spectrometer (JASCO, Easton, MD, USA) at 0.2 mg/ml from 190 to 240 nm. CD spectra were plotted using GraphPad Prism 5 (GraphPad Software Inc., La Jolla, CA, USA). CD spectra were analyzed by the SELCON3 (39, 40) and K2D3 (41) methods using the DichroWeb online analysis software (42, 43). Reference data sets 4 and 7 (range 190–240 nm) were used in the analyses (44).

V3 peptide binding assay

Biotinylated clade B V3 peptide was synthesized at the Structural Biology Core (University of Missouri, Columbia, MO, USA). The sequence (Biotin-GCRKRIHIGPGRAFYTC) was derived from MN V3 loop sequence (304–309, 312–319 based on HXB2 numbering). Peptide binding assays were performed in 96-well ½ area white plates (Perkin Elmer, Waltham, MA, USA) using a 40 μl reaction volume containing donor and acceptor beads (final concentration 20 μg/ml), 1× phosphate-buffered saline (PBS) pH 7.4, 0.01% Tween-20, and 0.1 mg/ml bovine serum albumin. A total of 200 nM N-terminal 6× histidine (His_6)-tagged scFv variants (50 nM final) were incubated with 400 nM biotinylated V3 peptide (100 nM final) for 1 h at room temperature. A total of 80 μg/ml of nickel chelated acceptor beads (Perkin Elmer, Waltham, MA, USA) were added to the wells and allowed to incubate for another hour in the dark before adding 80 μg/ml of streptavidin-coated donor beads (Perkin Elmer, Waltham, MA, USA). After 30 min incubation in the dark, the plates were analyzed using an EnSpire Plate Reader (Perkin Elmer, Waltham, MA, USA). Parental KD-247 scFv (wild-type, WT) was the positive control that gives high signal counts because of its strong binding to the clade B V3 peptide. A reaction containing only the peptide but no scFv served as the negative control. The signals of all the scFv variants were compared to the WT scFv signal. Statistical analyses were performed using 2-tailed 1-sample *t* test and Wilcoxon signed rank test at 95% confidence.

HIV-1 neutralization assay

Maraviroc, TZM-bl cells (from Dr. John C. Kappes, Dr. Xiaoyun Wu, and Tranzyme Inc., Durham, NC, USA), pSG3ΔEnv (from Drs. John C. Kappes and Xiaoyun Wu), pWT/BaL plasmid (Dr. Bryan Cullen), and H9/HTLV-III_{MN} NIH 1984 (Dr. Robert Gallo) were obtained through the U.S. NIH AIDS Reagent Program. The plasmid for expression of JR-FL Env (pCXN-JR-FL-Env) was from Dr. Shuzo Matsushita. TZM-bl cells were maintained in Dulbecco's modified Eagle's medium (DMEM) supplemented with 10% heat-inactivated fetal bovine serum (FBS), 100 units/ml penicillin, and 100 μg/ml streptomycin. The 293T cells were maintained in DMEM supplemented with 10% FBS, and penicillin/streptomycin. H9/HTLV-III_{MN} NIH 1984 was passaged in RPMI 1640 supplemented with L-glutamine and 10% FBS.

Replication-competent HIV-1_{BaL} and replication-deficient pseudotyped HIV-1 were produced by 293T transfection with pWT/BaL or pSG3ΔEnv and pCXN-JR-FL-Env plasmids (38). Replication-competent HIV-1_{MN} was obtained from supernatant of H9/HTLV-III_{MN} NIH 1984 culture (45, 46). Virus titers were determined using the previously described 50% tissue culture infectious dose ($TCID_{50}$) assay (47).The ability of KD-247 scFv variants to neutralize JR-FL Env pseudotyped HIV-1 was first evaluated. A total of 100 $TCID_{50}$ pseudotyped virus was preincubated with scFv variants (5 μM final concentration) (37°C) for 1 h before infecting TZM-bl cells (preseeded 1×10^4 cells/well). A total of 10 nM maraviroc (targets CCR5) was used as a positive control. Luciferase activity of infected TZM-bl cells was determined at 48 h postinfection using Bright-Glo Reagent (Promega, Madison, WI, USA). The relative infectivity was determined as ratio of the relative light units in the presence of scFv to virus control (PBS treated). The percentage of neutralization was calculated as 100 × (1 − relative infectivity). scFv variants that showed more than 50% neutralization were further studied as described above using HIV-1_{BaL} or HIV-1_{MN} in the presence of scFv at various concentrations to determine 50% neutralization concentration (EC_{50}). Data from at least three independent experiments were plotted using nonlinear regression equations in GraphPad Prism 5 software to obtain EC_{50} values.

RESULTS

KD-247 Fab crystal structure

The KD-247 Fab structure was determined to 1.55 Å, the highest resolution reported for any apo humanized antibody (**Fig. 1*A***). It was refined to an R-factor of 19% and an R_{free} of 21%. More than 98% of the KD-247 Fab residues had main chain torsion angles in the energetically favored regions of the Ramachandran plot (48), with no residues in disallowed regions (49) (Table 1). Using RBOW, the elbow angle of the KD-247 Fab was determined to be 127°, which falls within the range commonly observed for Fabs with κ light chains (50).

KD-247 is the first humanized anti-V3 mAb to be structurally characterized. The heavy and light chains were numbered using the Kabat numbering system (51, 52). The heavy and light chains are designated with an "H" and an "L", respectively. The CDR loops L1, L2, L3, H1, and H2 belong to canonical classes κ-3, 1, κ-1, 1, and 1 (53). The CDR H3 loop exhibits a kinked base conformation with the observation of the conserved hydrogen bond between the ring nitrogen of Trp^{H103}

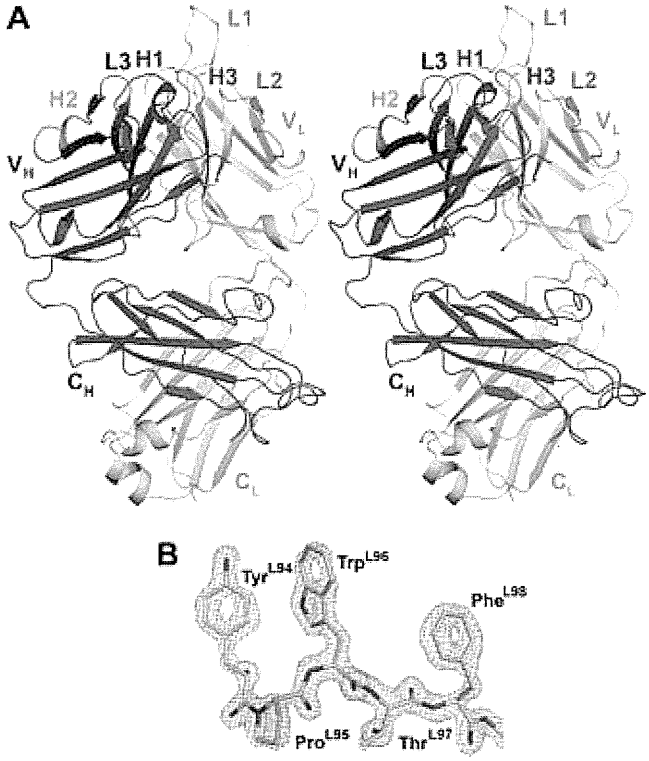

Figure 1. Crystal structure of KD-247 Fab. (A) Stereo view of the Fab including CDR regions (L1, cyan; L2, green; L3, blue; H1, red; H2, orange; H3, purple). Light and heavy chains are shown in light and dark gray. (B) *3Fo–2Fc* electron density map of light chain residues (σ = 2.0). All structural images were generated using PyMOL (*http://www.pymol.org/*).

and the carbonyl oxygen of Met^{H100A}; there is no salt bridge between Arg^{H94} and Asp^{H101} (54). Excellent electron density was continuous almost throughout the entire molecule (Fig. 1*B*), allowing assignment of partial occupancy and alternate conformations. Slightly disordered loops were observed for residues 42–43, 64–66, and 101–102 in the heavy chain but were included in the model.

The KD-247 Fab CDR L1 loop is very similar to the L1 loop from other Fabs, including the Fab of nonneutralizing HIV-1 antibody 13H11 (PDB ID: 3MNV; light chain RMSD compared to KD-247 light chain [$RMSD_L$] determined by PDBeFold = 0.62 Å), the Fab of a mAb that neutralizes human rhinovirus serotype 2 (PDB ID: 1BBD; $RMSD_L$ = 0.73 Å), an antitumor CH2-domain-deleted humanized antibody (PDB ID: 1ZA6; $RMSD_L$ = 0.55 Å), the Fab of human germ-line antibody 1-69/B3 (PDB ID: 3QOT; $RMSD_L$ = 0.44 Å), and the Fab of *Mus musculus* germ-line antibody S25-2 (PDB ID: 1Q9K; $RMSD_L$ = 0.65 Å) (**Fig. 2*A***). The CDR L1 loop is considerably longer in the KD-247 Fab (17 residues long) than what is observed for other anti-V3 loop antibodies, including murine antibody 83.1 (PDB ID: 1NAK) and human antibodies F425-B4e8 (2QSC), 2219 (2B0S), and 1006-15D (3MLW) (Fig. 2*B*). The CDR L1 loop of anti-V3 loop murine antibody 83.1 (PDB ID: 1NAK) is 16 residues long but is bent in the crystal structure to avoid crystal packing clashes with residues from the variable heavy chain of a symmetry-related molecule (55).

We pursued cocrystallization of the KD-247 Fab in complex with various V3 peptides of different sequences and lengths, which resulted in many beautiful crystals but poor X-ray diffraction or internal lattice problems that could not be resolved. The crystal packing of the apo Fab does not allow room for the peptide to bind through soaking experiments. Thus, we constructed a molecular model of the KD-247 Fab in complex with the V3 loop in order to understand the molecular details of HIV-1 clade B V3 loop recognition by KD-247.

Superposition of the V3 loop

In our model of the KD-247 Fab crystal structure in complex with a clade B V3 Gly^{312}-Pro^{313}-Gly^{314}-Arg^{315} (GPGR)-containing peptide, the V3 residues are designated with a "P" and numbered according to the HXB2 sequence (56). We aligned previously determined Fab-V3 complexes to KD-247 Fab. The V3 peptides of many Fab-V3 complexes that aligned with the KD-247 Fab did not fit well after superposition with the KD-247 binding pocket. One exception was the V3 peptide from 2QSC, derived from MN and called RP142 (Y^{P301}NKRKRIHI^{P309} G^{P312}PGRAFYTTKNIIGC^{P326}) (57, 58).

The RP142 peptide fits nicely into the binding pocket, with only minor obstructions. The side chains of Ile^{P309} and Tyr^{P318} and the main chain of Phe^{P317} in V3 were in close contact (<2.0 Å) with the Trp^{H33}, Asn^{H58}, and Tyr^{L94} side chains of KD-247 Fab. After minimization, the positions of the important GPGR residues were virtually unchanged. The primary interactions between the RP142 peptide and the KD-247 Fab involve the V3 arch of the loop and the CDR L1 and L3 regions (Fig. 2*C*). Previous studies have shown that the characteristic observed interactions between anti-V3 Fabs with the V3 peptides occur in the long extended CDR H3 (59–61). In our case and in the 2QSC structure, Arg^{315} of the V3 loop interacts with light chain Fab residues. The most interesting interaction occurs between Arg^{315} of the RP142 peptide and KD-247 Tyr^{L32} and Tyr^{L92} (Fig. 2*D*). Arg^{315} appears to be stabilized by van der Waals interactions with the side chains of the two tyrosines and additionally by a hydrogen bond with the phenoxy group of Tyr^{L92}. The arginine is also further stabilized by a hydrogen bond with Asn^{L27d}. An intricate hydrogen bond network between CDR L1 loop residues Tyr^{L32}, Asp^{L28}, and Asn^{L27d} helps to stabilize Tyr^{L32} and Asn^{L27d} in positions to interact with Arg^{315} (Fig. 2*D*).

G314E and R315K KD-247-resistant V3 peptides with KD-247

Two mutations in the V3 arch confer KD-247 resistance. HIV-$1_{JR\text{-}FL}$ with G314E was neutralized 16-fold less efficiently by KD-247 than HIV-$1_{JR\text{-}FL}$ without this mutation (62). An HIV-1_{BaL} variant containing a potential *N*-linked glycosylation site (PNGS) insertion in V2 and an R315K mutation in the V3 arch provided a very high resistance phenotype to KD-247 (63). The long Glu

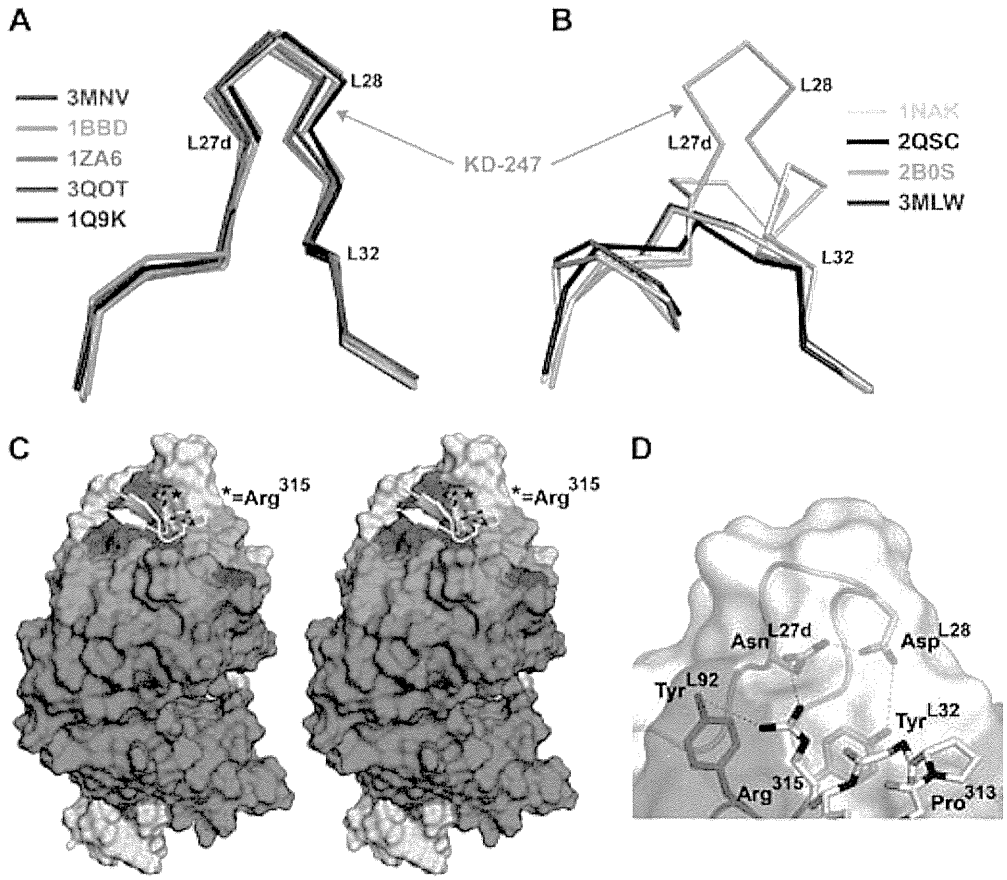

Figure 2. Structural comparison of KD-247 with other Fabs and potential interactions with a V3 peptide. (A) Similarities of the KD-247 CDR L1 loop (cyan) to other Fabs (PDB ID: 3MNV, red; 1BBD, orange; 1ZA6, green; 3QOT, magenta; 1Q9K, blue). The RMSD between the light chain of all Fabs and KD-247 is <0.75 Å. (B) The KD-247 CDR L1 loop (cyan) is unique from other anti-V3 mAbs (PDB ID: 1NAK, yellow; 2QSC, gray; 2B0S, pink; 3MLW, brown). (C) Stereo view of KD-247 (surface representation, colors as in Fig. 1) with the RP142 peptide (white cartoon/yellow sticks) modeled in the binding pocket. (D) Interactions between Arg^{315} of the RP142 peptide, Tyr^{L32} and Asn^{L27d} of CDR L1 (cyan) and Tyr^{L92} of CDR L3 (blue; dashed lines are H bonds). Tyr^{L32} is stabilized by an H-bond network that includes Asp^{L28} and Asn^{L27d} of CDR L1.

chain in G314E V3 causes steric clashes with KD-247 CDR L1, L2, and H3 (data not shown). Similarly, R315K also creates steric clashes with CDR L1 and L3 of KD-247.

KD-247 scFv variants

On the basis of our KD-247 structure-guided model, we designed KD-247 variants in a smaller size 30 kDa scFv antibody format. scFv variants with single or double Ala substitutions at Asn^{L27d}, Tyr^{L32}, and/or Tyr^{L92} were generated to disrupt the proposed interactions. To understand the proposed interactions of Tyr^{L32} and Tyr^{L92} with Arg^{315}, we generated scFv variants with Phe substitutions at these positions. Additional substitutions at Asn^{L27d}, Tyr^{L32}, and Tyr^{L92} were generated to further understand the effects of side chains on the KD-247 interactions with the GPGR V3 arch. We proposed that substitution with polar side chain of Asn or Gln at Asn^{L27d}, Tyr^{L32}, and Tyr^{L92} will maintain affinity for Arg^{315}. Substitution with the long basic side chain of Arg and Lys or the short acidic side chain of Asp and Glu at Asn^{L27d}, Tyr^{L32}, and Tyr^{L92} of KD-247 may provide additional insights into the interactions with the GPGR V3 arch.

All scFv variants were expressed and purified by a stepwise refolding process (38) (Supplemental Fig. 1*A*) that overcomes the previously reported challenge of obtaining anti-V3 loop scFvs (64). Despite the low recovery of refolded monomeric scFvs, we were able to obtain sufficient quantities for the subsequent analyses. A correctly folded scFv should retain an immunoglobulin-like structure with each variable domain consisting of nine antiparallel β-sheets (65). We previously used CD spectroscopy to confirm efficient refolding of WT KD-247 scFv (38). Here, we used far-UV CD spectroscopy to analyze the folding of mutant KD-247 scFv variants (Supplemental Fig. 1*B–E*). Protein folding can be assessed from the CD ellipticity value (*y* axis intercept): unordered protein structure increases with decreasing ellipticity value at short wavelength (200 nm) (66). Overall, the scFvs were better folded in the presence of a 16mer HIV-1_{MN}-derived V3 peptide (Supplemental Fig. 1*B–E*; *cf.* right *vs.* left panels). Folding was further confirmed by analyzing the CD data using the SELCON3 (39, 40) and K2D3 (41) methods in the DichroWeb online analysis software (data not shown) (42, 43). Generally, the quantification of the CD data by SELCON3 and K2D3 confirm that the secondary structure of the Asn^{L27d} scFv variants had a comparable β-sheet content to that of WT scFv (Supplemental Fig. 1*B*). Of the Tyr^{L92} variants, results from the K2D3 method demonstrated that Phe^{L92}, Gln^{L92}, and Arg^{L92} showed the most comparable β-sheet content to WT scFv, which is again consistent with the CD spectra (Supplemental Fig. 1*B*). The results from the SELCON3 and K2D3 methods showed that Tyr^{L32} variants and the double mutants Y32A/Y92A and N27dA/Y32A exhibited lower β-sheet contents compared with WT scFv, which demonstrates poor folding in agreement with the CD spectra (Supplemental Fig. 1*D, E*). This observation indicated that the Tyr^{L32} aromatic ring is required for proper conformation of KD-247 when purified *in vitro*. We selected scFv variants

that showed a proper β-sheet profile for further investigation of the KD-247 scFv-V3 loop interactions.

scFv–V3 loop interactions

To compare binding of KD-247 scFv variants to GPGR V3 loop peptides, we performed a protein–protein interaction assay using the AlphaScreen technology (67). The streptavidin-coated donor beads and the nickel-chelate acceptor beads bind to the biotinylated V3 peptides and the purified His_6-tagged scFvs, respectively. A favorable interaction between the V3 loop peptide and the scFv variant brings the 2 types of fluorophore-coated beads into proximity, and an amplified light signal is generated upon excitation (**Fig. 3*A***). Our results showed that similar to WT scFv, several scFv variants, including N27dD, N27dE, N27dK, N27dR, Y92A, Y92F, Y92R, and Y32F, interact with the clade B V3 loop peptide, and the signals measured were significantly different from the no-scFv negative control (Fig. 3*B*).

In addition to measuring the binding interactions of scFv with cyclic V3 loop peptides, we also determined their ability to neutralize the infectivity of pseudotyped HIV-1 (HIV-$1_{JR\text{-}FL}$, **Table 2**) that contains a V3 loop similar to the one used in the modeling studies (HIV-1_{MN}-derived RP142 peptide). Only WT KD-247 Fab and scFv, as well as N27dD and Y92F scFvs, could neutralize by at least 80% pseudotyped clade B HIV-1 using 5 μM scFv (Fig. 3*C*). Other scFv variants, which initially showed binding to the clade B GPGR V3 loop peptide (Fig. 3*B*), neutralized less than 30% of pseudotyped HIV-1 under the same conditions (Fig. 3*C*).

We also determined the EC_{50} of the most potent scFvs in TZM-bl neutralization assays using fully infectious CCR5-tropic HIV-1_{BaL} and CXCR4-tropic HIV-1_{MN} (**Table 3**). Similarly, the refolded WT scFv neutralized the replication-competent HIV-1_{MN} and HIV-1_{BaL} at comparable EC_{50} values (0.7 and 0.6 μM, respectively). Y92F scFv showed similar EC_{50} values compared to WT scFv (0.8 μM for HIV-1_{MN} and 0.5 μM for HIV-1_{BaL}), suggesting that the aromatic interaction with this residue is crucial. A slight increase in the EC_{50} of N27dD scFv (2.1 μM for HIV-1_{MN} and 1.2 μM for HIV-1_{BaL}), indicated that Asn^{L27d} is better at stabilizing the interaction with Arg^{315}. These results provided insights into the interactions of Arg^{315} with side chains at the interface of the KD-247 light chain.

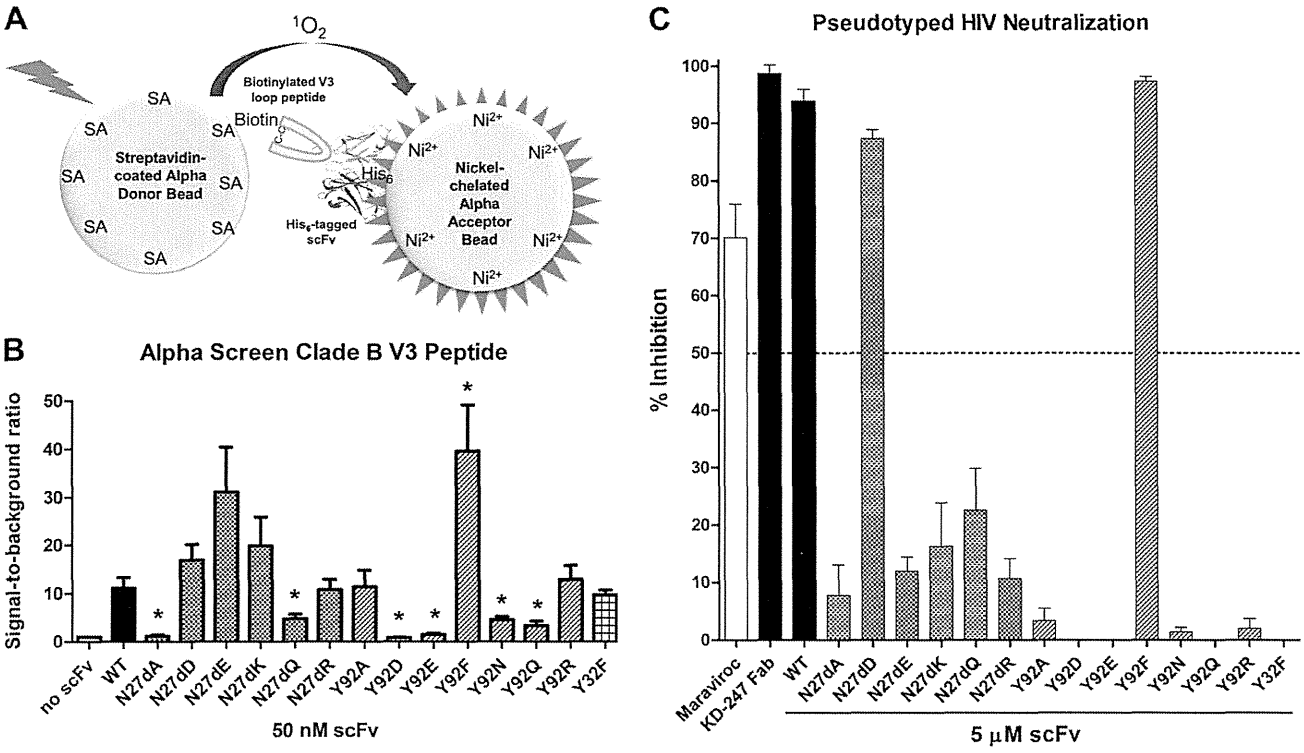

Figure 3. Interactions of scFv variants with V3 loop. (A) Schematic representation of KD-247 scFv interactions with a V3 peptide using AlphaScreen technology. His-tagged scFvs were allowed to interact with biotinylated V3 peptide. The interaction was detected using nickel (Ni^{2+})-chelated AlphaScreen acceptor beads and streptavidin (SA)-coated AlphaScreen donor beads. (B) Interaction of scFv variants with cyclic clade B V3 peptide. Results are expressed as the means of signal-to-background ratio from 3 independent experiments. Error bars indicate SEM. Statistically significant differences compared to WT scFv are represented by an asterisk ($*P < 0.05$). (C) Neutralization assay of HIV-1 Env pseudotyped virus on TZM-bl cells. A total of 10 nM maraviroc (CCR5 antagonist) or 5 μM KD-247 Fab or His-tagged scFv variants were preincubated with HIV-$1_{JR\text{-}FL}$ Env pseudotyped HIV-1 before infection of TZM-bl. Luminescence was measured 48 h after infection to determine scFv variants that result in >50% neutralization of pseudotyped virus. Results are represented as the average of percentage neutralization relative to virus control from at least three experiments; error bars indicate SEM.

TABLE 2. *V3 loop sequences of clade B HIV-1 strains*

HIV-1 strain	Tropism	V3 loop sequence
MN	X4	CTRPNYNKRKRIHIGPGRAFYTTKNIKGTIRQAHC
BaL	R5	-----N-T--S--------L---GE-I-D------
JR-FL	R5	-----N-T--S------------GE-I-D------

Dashes indicate identical amino acid residue.

DISCUSSION

The V3 loop of HIV-1 gp120 is flexible and structurally diverse, as evidenced by the wide range of different conformations of Arg^{315} observed in gp120 and Fab/V3 complexes (aligned GPGR arches shown in **Fig. 4*A***). This diverse loop, and specifically Arg^{315}, which correlates with genotypic specificity, is also recognized in a variety of ways by anti-V3 mAbs. Although most mAbs interact with their respective antigen through heavy chain interactions (68), several anti-V3 mAbs interact with Arg^{315} through residues of their light chains. For example, murine Fab 83.1 interacts with Arg^{315} through hydrogen bond between the main and side chains of Thr^{L91} (55) (Fig. 4*B*). Human Fab 2219 recognizes Arg^{315} through a hydrogen bond with Asn^{L31} (69) (Fig. 4*C*). In the human F425-B4e8 Fab/V3 complex, Arg^{315} is sandwiched between residues Tyr^{L32} and Asp^{L92} and is stabilized by a salt bridge with Asp^{L92}, as well as hydrogen bonds with the main and side chains of Asp^{L92} (58) (Fig. 4*D*). Additionally, Arg^{315} interacts with the human 1006-15D Fab through hydrogen bonds with the side chains of Asn^{L30} and Asp^{L93} (60) (Fig. 4*E*). KD-247 also uses its light chain to recognize Arg^{315}, but in what appears to be a different manner than other anti-V3 mAbs: in addition to hydrogen bond interactions with Tyr^{L92} and van der Waals interactions with Tyr^{L32} and Tyr^{L92}, Asn^{L27d} also forms a hydrogen bond with the Arg^{315} side chain, providing additional stability. Asn^{L27d} and Tyr^{L32} are held in place by an elaborate hydrogen bond network also involving Asp^{L28} (Fig. 2*D*). These distinct interactions involve the unique CDR L1 insertion of KD-247 and provide a plausible answer for why Arg^{315} is needed for HIV-1 neutralization by KD-247.

The interactions between mAbs and the V3 loop are also affected by the use of different CDRs. For example, the human mAb 537-10D recognizes the same IGPGR epitope as KD-247, yet it uses a long insertion in the CDR H3 loop to make nonspecific interactions with the V3 loop in the form of a 4-stranded antiparallel β-sheet (**Fig. 5*A***), in comparison to KD-247, which primarily uses CDR L1 for V3 loop interactions (Fig. 5*B*, *C*). Although they recognize the same epitope, 537-10D demonstrates a narrow HIV-1 neutralization profile

TABLE 3. *Fifty percent neutralization concentration (EC_{50}) (μM) against clade B HIV-1*

Assay	HIV-1_{MN}(CXCR4-tropic)	HIV-1_{BaL}(CCR5-tropic)
Maraviroc	>0.1	0.002 ± 0.001
KD-247 Fab	0.2 ± 0.06	0.1 ± 0.02
KD-247 scFv	0.7 ± 0.2	0.6 ± 0.1
N27dD scFv	2.1 ± 0.7	1.2 ± 0.2
Y92F scFv	0.8 ± 0.08	0.5 ± 0.09

Data represent the mean ± SD from the results of three independent experiments.

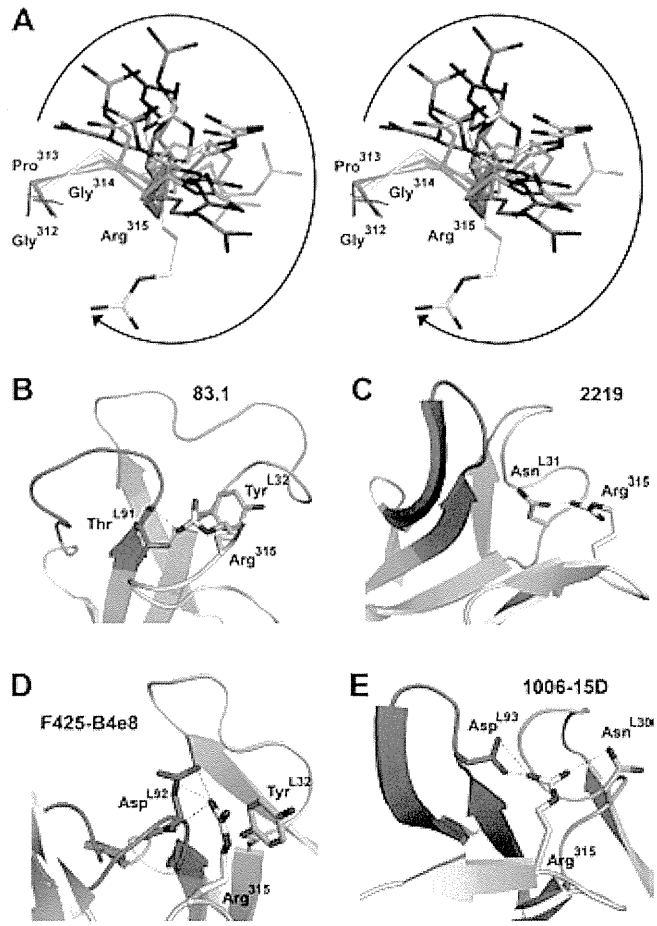

Figure 4. Structural variability of Arg^{315} and recognition by anti-V3 mAb light chains. (A) Stereo view of "GPGR"-containing V3 loops in the following: 58.2 Fab complexes (PDB ID: 1F58, red; 2F58, green; 3F58, magenta), 83.1 Fab complex (1NAK, yellow); 447-52D (1Q1J, orange); 2219 Fab complex (2B0S, pink); F425-B4e8 Fab complex (2QSC, dark gray); 268-D Fab complex (3GO1, gray); 1006-15D Fab complex (3MLW, brown); 3074 Fab complex (3MLX, blue); 2557 Fab complexes (3MLR, light green; 3MLT, cyan); 2558 Fab complex (3UJI, mauve); 537-10D Fab complex (3GHE, hot pink); the V3 loop from the X5 Ab complex with JR-FL gp120 and CD4 (2B4C, dark green); and the V3 loop from the sulfated-tyrosine 412d Ab complex with YU2 gp120 and CD4 (2QAD, light blue). Arrow indicates the space occupied by Arg^{315} conformations in the various structures. Arg^{315} is also stabilized by interactions with light chain residues in some mAbs, including 83.1 (B), 2219 (C), F425-B4e8 (D), and 1006-15D (E). H bonds and salt bridges are shown as black and red dashed lines.

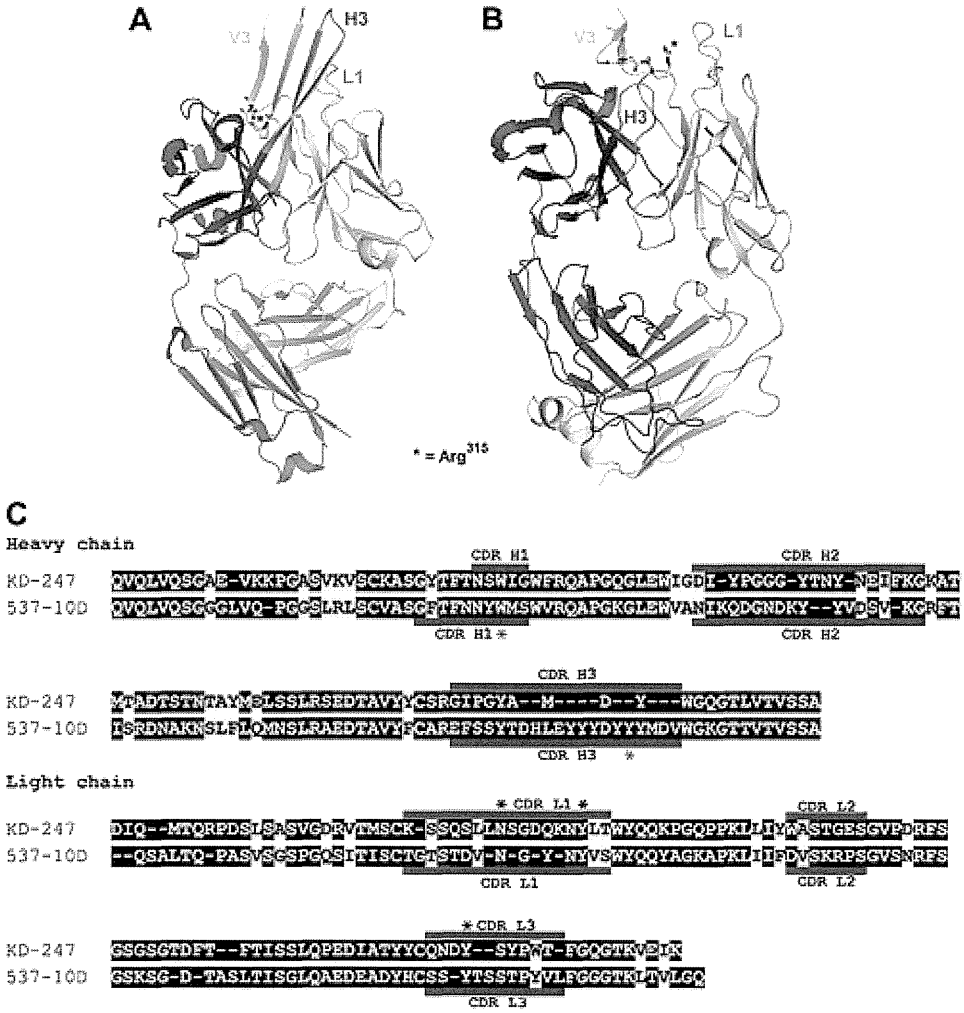

Figure 5. The 537-10D and KD-247 target the same IGPGR epitope using different modes of V3 binding. (A) 537-10D Fab (heavy and light chains in dark and light gray) in complex with an MN V3 peptide (yellow, PDB ID: 3GHE). The primary binding interactions occur in the CDR H3 loop (purple). (B) KD-247 Fab bound to the RP142 V3 peptide (same colors as in (A)). Most of the binding interactions occur in the CDR L1 loop (cyan). (C) Sequence alignment of the KD-247 and 537-10D variable regions (CDR regions in red). Identical residues are highlighted in blue and similar residues in yellow. Asterisks mark the residues making interactions with Arg^{315} of the RP142 V3 peptide. Sequence alignment was performed by the Sequence Manipulation Suite (*http://www.bioinformatics.org/sms2/index.html*). CDRs were labeled on the basis of previously published sequences (27, 59).

compared to KD-247 (70). This is likely due in part to the more restricted antigen binding site of 537-10D, in which the Trp^{H33}, Glu^{H95}, and Tyr^{H100J} residues that interact with Arg^{315} of the V3 loop are buried in a deep pocket (~6Å) that requires a close fit to bind the V3 loop. The CDR region of KD-247 demonstrates a shallow binding pocket that may be able to better tolerate flexibility of the V3 arch (59).

Resistance mutations at gp120 affect interactions between mAb and V3 loop and help HIV-1 escape neutralizing antibodies. Two mutations in the V3 arch region of gp120 cause resistance to KD-247. KD-247 neutralizes $HIV\text{-}1_{JR\text{-}FL}$ with a G314E mutation ~20-fold less efficiently than WT (62), and also binds 100× weaker than WT to $HIV\text{-}1_{BaL}$ with a V2 PNGS insertion in addition to the V3 R315K mutation (63). Our modeling studies suggest that mutation from Gly to Glu at 314 and from Arg to Lys at 315 creates steric interactions with the binding pocket of KD-247 (data not shown). These steric contacts likely affect KD-247 binding to V3 loops containing these mutations and may explain the reported differences in KD-247 binding and HIV-1 neutralization.

Our proposed interactions were validated by the generated scFv variants and the results of our binding and neutralization assays. The data suggest that KD-247 uses an elaborate network of interactions that are based on the long insertion in CDR L1 and involve residues Asn^{L27d}, Asp^{L28}, Tyr^{L32}, and Tyr^{L92} (Fig. 2*D*). Importantly, one of these residues (Tyr^{L32}) appears to be important for proper scFv folding, as almost all of the mutants at this position were inactive in neutralization assays (Fig. 3*C*) and poorly folded (CD spectra in Supplemental Fig. 1*D*). Phe^{L32} was the only mutant at position 32 that demonstrated proper scFv folding. Although variant Phe^{L32} demonstrated some binding activity to the V3 loop peptide (Fig. 3*B*), it did not neutralize pseudotyped clade B HIV-1 (Fig. 3*C*). Hence, an aromatic residue at position 32 in the light chain is important for proper scFv folding but not necessarily for neutralization, where it seems that the phenoxy group is critical. Changes at position 27d do not affect scFv folding (Supplemental Fig. 1*B*) and appear to either have limited effect (with the exception of Ala^{L27d} and Gln^{L27d}) or even enhance binding to the V3 loop (Fig. 3*B*). The loss of V3 loop binding and neutralization ability of the Ala^{L27d} KD-247 scFv variant is consistent with the proposed role of Asn^{L27} in interacting with Arg^{315}. However, the only variant that was able to efficiently neutralize pseudotyped clade B HIV-1 was Asp^{L27d} (Fig. 3*C*). It is likely that the Glu^{L27d} and Gln^{L27d} variants are not as efficient in neutralization of pseudotyped virus because of their longer side chains

(as compared to Asp^{L27d} and Asn^{L27d}). Similarly, the even longer side chains of Arg^{L27d} and Lys^{L27d} are likely to negatively affect interactions with Arg^{315} because of steric constraints. The ability of the N27dD variant to neutralize clade B HIV-1 suggests that KD-247 may be substituted with Asp^{L27d} to retain activity against clade B HIV. This substitution would still be able to participate in the intricate network of hydrogen bond interactions proposed in our model for recognition of Arg^{315}. Although many of the scFv variants at position 92 of the light chain demonstrated proper folding (Supplemental Fig. 1*C*), Phe^{L92} demonstrated enhanced binding to the clade B V3 loop peptide while Ala^{L92} and Arg^{L92} had similar binding compared to the WT scFv (Fig. 3*B*), but only Phe^{L92} showed effective neutralization of clade B HIV-1 Env pseudotyped virus (Fig. 3*C*). These results establish that the aromatic ring at Tyr^{L92} is essential for clade B V3 loop recognition. Overall, these observations highlight the importance of Asn^{L27d}, Tyr^{L32}, and Tyr^{L92} in neutralizing clade B HIV-1 containing a GPGR V3 loop arch. Importantly, these results reveal that binding of scFv variants to clade B V3 loop peptides does not necessarily correlate with efficient HIV-1 clade B neutralization. It is possible that other factors may affect binding of the antibody in the context of the full Env glycoprotein that do not factor in to V3 peptide binding. The recent crystal structure of the native Env trimer by Julien *et al.* (71) revealed that the gp120 subunits are stabilized by β-hairpin interactions of the V3 loop and the V1/V2 strands B and C near the top of the trimer. The arch of the V3 loop is hidden by an *N*-acetyl glucosamine from the Asn^{197} glycan at the C-terminal region of V2 strand D from a neighboring protomer. This glycan blocks access to the V3 arch and may affect mAb binding.

Our findings are in agreement with previous work highlighting the dramatic flexibility of V3 loop and underscore the challenges in engineering antibodies that will be useful for treatment and vaccine design. Antibody engineering based on the interactions reported in our and other structures may lead to enhanced interactions with both Arg and Gln residues at position 315 of the V3 loop. For example, we expect that mutations of KD-247 residue Asn^{L27d} to longer polar residues (N27dQ, N27dK, and N27dR) should maintain the hydrogen bond interaction with clade B Arg^{315} and also be able to hydrogen bond with the shorter non–clade B Gln^{315}. Additionally, mutations of KD-247 residue Asp^{L28} to long polar residues (D28K, D28R, and D28E) should reach and interact with both clade B Arg^{315} and non–clade B Gln^{315}. Similarly, the Y32R mutant should maintain van der Waals interactions with clade B Arg^{315} and also make hydrogen bond interactions with non–clade B Gln^{315}. Combinations of the above mutations in the 27d, 28, 32, and 92 positions of the light chain of KD-247 may also help to maintain interactions with Arg^{315} and improve interactions with Gln^{315}. Additional approaches may include mutations of other KD-247 residues that do not interact directly with residue 315 of the V3 loop. Such interactions are observed in the structures of the 2557 and 3074 Fabs (22, 60) in complex with the V3 loop. Finally, extended CDR H3 loops may be designed to make nonspecific main chain interactions with the V3 loop, as is the case with 447-52D (61) and 537-10D (59), which form three-stranded and four-stranded antiparallel β-sheets with the V3 loop target.

Although the propensity of V3 loop to serve as an immunogen to elicit broadly neutralizing antibodies against HIV-1 of multiple clades has been challenging, the extensive studies performed by the Zolla-Pazner, Górny, Wilson, and Kong groups suggest that this strategy may be achievable (22, 25, 55, 58–61, 69, 70, 72). FJ

The authors thank Dr. Jay Nix of ALS beamline 4.2.2 for assistance with data collection. The Advanced Light Source is supported by the director of the Office of Science, Office of Basic Energy Sciences, U.S. Department of Energy, under contract DE-AC02-05CH11231. A portion of the crystal structure of the unliganded KD-247 Fab was solved with guidance provided at the workshop entitled "CCP4 School: From Data Processing to Structure Refinement and Beyond" at Argonne National Laboratory (*http://www.ccp4.ac.uk/schools/APS-2008/index.php*) attended by K.A.K. The authors thank Drs. Krishna K. Sharma and Puttur Santhoshkumar for assistance with CD data collection. This work was supported, in whole or in part, by U.S. National Institutes of Health Grants AI076119, AI094715, AI099284, AI100890, AI112417, and GM103368 (S.G.S.). We also acknowledge support from the Ministry of Knowledge and Economy, Bilateral International Collaborative R&D Program, Republic of Korea. L.A.C. is supported by the MU-HHMI C^3 Program. B.M. is a recipient of the amfAR Mathilde Krim Fellowship and a Canadian Institutes of Health Research Fellowship.

REFERENCES

1. Le Douce, V., Janossy, A., Hallay, H., Ali, S., Riclet, R., Rohr, O., and Schwartz, C. (2012) Achieving a cure for HIV infection: do we have reasons to be optimistic? *J. Antimicrob. Chemother.* **67**, 1063–1074
2. Wei, X., Decker, J. M., Wang, S., Hui, H., Kappes, J. C., Wu, X., Salazar-Gonzalez, J. F., Salazar, M. G., Kilby, J. M., Saag, M. S., Komarova, N. L., Nowak, M. A., Hahn, B. H., Kwong, P. D., and Shaw, G. M.(2003) Antibody neutralization and escape by HIV-1. *Nature* **422**, 307–312
3. Parren, P. W., Burton, D. R., and Sattentau, Q. J. (1997) HIV-1 antibody—debris or virion? *Nat. Med.* **3**, 366–367
4. Yusim, K., Korber, B. T. M., Brander, C., Barouch, D., de Boer, R., Haynes, B. F., Koup, R., Moore, J. P., Walker, B. D., and Watkins, D. I. (2011) HIV Molecular Immunology, Los Alamos National Laboratory, Theoretical Biology and Biophysics, Los Alamos, New Mexico, http://www.hiv.lanl.gov/content/immunology
5. Burton, D. R., Barbas III, C. F., Persson, M. A., Koenig, S., Chanock, R. M., and Lerner, R. A. (1991) A large array of human monoclonal antibodies to type 1 human immunodeficiency virus from combinatorial libraries of asymptomatic seropositive individuals. *Proc. Natl. Acad. Sci. USA* **88**, 10134–10137
6. Trkola, A., Purtscher, M., Muster, T., Ballaun, C., Buchacher, A., Sullivan, N., Srinivasan, K., Sodroski, J., Moore, J. P., and Katinger, H. (1996) Human monoclonal antibody 2G12 defines a distinctive neutralization epitope on the gp120 glycoprotein of human immunodeficiency virus type 1. *J. Virol.* **70**, 1100–1108
7. Stiegler, G., Kunert, R., Purtscher, M., Wolbank, S., Voglauer, R., Steindl, F., and Katinger, H. (2001) A potent cross-clade neutralizing human monoclonal antibody against a novel epitope on gp41 of human immunodeficiency virus type 1. *AIDS Res. Hum. Retroviruses* **17**, 1757–1765
8. Barbato, G., Bianchi, E., Ingallinella, P., Hurni, W. H., Miller, M. D., Ciliberto, G., Cortese, R., Bazzo, R., Shiver, J. W., and Pessi, A. (2003) Structural analysis of the epitope of the anti-HIV antibody 2F5 sheds light into its mechanism of neutralization and HIV fusion. *J. Mol. Biol.* **330**, 1101–1115

9. Walker, L. M., Phogat, S. K., Chan-Hui, P. Y., Wagner, D., Phung, P., Goss, J. L., Wrin, T., Simek, M. D., Fling, S., Mitcham, J. L., Lehrman, J. K., Priddy, F. H., Olsen, O. A., Frey, S. M., Hammond, P. W.; Protocol G Principal Investigators, Kaminsky, S., Zamb, T., Moyle, M., Koff, W. C., Poignard, P., and Burton, D. R. (2009) Broad and potent neutralizing antibodies from an African donor reveal a new HIV-1 vaccine target. *Science* **326**, 285–289
10. Wu, X., Yang, Z. Y., Li, Y., Hogerkorp, C. M., Schief, W. R., Seaman, M. S., Zhou, T., Schmidt, S. D., Wu, L., Xu, L., Longo, N. S., McKee, K., O'Dell, S., Louder, M. K., Wycuff, D. L., Feng, Y., Nason, M., Doria-Rose, N., Connors, M., Kwong, P. D., Roederer, M., Wyatt, R. T., Nabel, G. J., and Mascola, J. R. (2010) Rational design of envelope identifies broadly neutralizing human monoclonal antibodies to HIV-1. *Science* **329**, 856–861
11. Walker, L. M., Huber, M., Doores, K. J., Falkowska, E., Pejchal, R., Julien, J. P., Wang, S. K., Ramos, A., Chan-Hui, P. Y., Moyle, M., Mitcham, J. L., Hammond, P. W., Olsen, O. A., Phung, P., Fling, S., Wong, C. H., Phogat, S., Wrin, T., Simek, M. D., Protocol G Principal Investigators, Koff, W. C., Wilson, I. A., Burton, D. R., and Poignard, P. (2011) Broad neutralization coverage of HIV by multiple highly potent antibodies. *Nature* **477**, 466–470
12. Scheid, J. F., Mouquet, H., Ueberheide, B., Diskin, R., Klein, F., Oliveira, T. Y., Pietzsch, J., Fenyo, D., Abadir, A., Velinzon, K., Hurley, A., Myung, S., Boulad, F., Poignard, P., Burton, D. R., Pereyra, F., Ho, D. D., Walker, B. D., Seaman, M. S., Bjorkman, P. J., Chait, B. T., and Nussenzweig, M. C. (2011) Sequence and structural convergence of broad and potent HIV antibodies that mimic CD4 binding. *Science* **333**, 1633–1637
13. Huang, J., Ofek, G., Laub, L., Louder, M. K., Doria-Rose, N. A., Longo, N. S., Imamichi, H., Bailer, R. T., Chakrabarti, B., Sharma, S. K., Alam, S. M., Wang, T., Yang, Y., Zhang, B., Migueles, S. A., Wyatt, R., Haynes, B. F., Kwong, P. D., Mascola, J. R., and Connors, M. (2012) Broad and potent neutralization of HIV-1 by a gp41-specific human antibody. *Nature* **491**, 406–412
14. Checkley, M. A., Luttge, B. G., and Freed, E. O. (2011) HIV-1 envelope glycoprotein biosynthesis, trafficking, and incorporation. *J. Mol. Biol.* **410**, 582–608
15. Berger, E. A., Murphy, P. M., and Farber, J. M. (1999) Chemokine receptors as HIV-1 coreceptors: roles in viral entry, tropism, and disease. *Annu. Rev. Immunol.* **17**, 657–700
16. Javaherian, K., Langlois, A. J., McDanal, C., Ross, K. L., Eckler, L. I., Jellis, C. L., Profy, A. T., Rusche, J. R., Bolognesi, D. P., Putney, S. D., et al. (1989) Principal neutralizing domain of the human immunodeficiency virus type 1 envelope protein. *Proc. Natl. Acad. Sci. USA* **86**, 6768–6772
17. Matsushita, S., Robert-Guroff, M., Rusche, J., Koito, A., Hattori, T., Hoshino, H., Javaherian, K., Takatsuki, K., and Putney, S. (1988) Characterization of a human immunodeficiency virus neutralizing monoclonal antibody and mapping of the neutralizing epitope. *J. Virol.* **62**, 2107–2114
18. Rusche, J. R., Javaherian, K., McDanal, C., Petro, J., Lynn, D. L., Grimaila, R., Langlois, A., Gallo, R. C., Arthur, L. O., Fischinger, P. J., et al. (1988) Antibodies that inhibit fusion of human immunodeficiency virus-infected cells bind a 24-amino acid sequence of the viral envelope, gp120. *Proc. Natl. Acad. Sci. USA* **85**, 3198–3202
19. Lynch, R. M., Shen, T., Gnanakaran, S., and Derdeyn, C. A. (2009) Appreciating HIV type 1 diversity: subtype differences in Env. *AIDS Res. Hum. Retroviruses* **25**, 237–248
20. Gorny, M. K., Williams, C., Volsky, B., Revesz, K., Cohen, S., Polonis, V. R., Honnen, W. J., Kayman, S. C., Krachmarov, C., Pinter, A., and Zolla-Pazner, S. (2002) Human monoclonal antibodies specific for conformation-sensitive epitopes of V3 neutralize human immunodeficiency virus type 1 primary isolates from various clades. *J. Virol.* **76**, 9035–9045
21. Pantophlet, R., Aguilar-Sino, R. O., Wrin, T., Cavacini, L. A., and Burton, D. R. (2007) Analysis of the neutralization breadth of the anti-V3 antibody F425-B4e8 and re-assessment of its epitope fine specificity by scanning mutagenesis. *Virology* **364**, 441–453
22. Hioe, C. E., Wrin, T., Seaman, M. S., Yu, X., Wood, B., Self, S., Williams, C., Gorny, M. K., and Zolla-Pazner, S. (2010) Anti-V3 monoclonal antibodies display broad neutralizing activities against multiple HIV-1 subtypes. *PLoS ONE* **5**, e10254
23. Conley, A. J., Gorny, M. K., Kessler II, J. A., Boots, L. J., Ossorio-Castro, M., Koenig, S., Lineberger, D. W., Emini, E. A., Williams, C., and Zolla-Pazner, S. (1994) Neutralization of primary human immunodeficiency virus type 1 isolates by the broadly reactive anti-V3 monoclonal antibody, 447-52D. *J. Virol.* **68**, 6994–7000
24. Gorny, M. K., Conley, A. J., Karwowska, S., Buchbinder, A., Xu, J. Y., Emini, E. A., Koenig, S., and Zolla-Pazner, S. (1992) Neutralization of diverse human immunodeficiency virus type 1 variants by an anti-V3 human monoclonal antibody. *J. Virol.* **66**, 7538–7542
25. Gorny, M. K., Williams, C., Volsky, B., Revesz, K., Wang, X. H., Burda, S., Kimura, T., Konings, F. A., Nádas, A., Anyangwe, C. A., Nyambi, P., Krachmarov, C., Pinter, A., and Zolla-Pazner, S. (2006) Cross-clade neutralizing activity of human anti-V3 monoclonal antibodies derived from the cells of individuals infected with non-B clades of human immunodeficiency virus type 1. *J. Virol.* **80**, 6865–6872
26. van Gils, M. J., and Sanders, R. W. (2013) Broadly neutralizing antibodies against HIV-1: templates for a vaccine. *Virology* **435**, 46–56
27. Eda, Y., Takizawa, M., Murakami, T., Maeda, H., Kimachi, K., Yonemura, H., Koyanagi, S., Shiosaki, K., Higuchi, H., Makizumi, K., Nakashima, T., Osatomi, K., Tokiyoshi, S., Matsushita, S., Yamamoto, N., and Honda, M. (2006) Sequential immunization with V3 peptides from primary human immunodeficiency virus type 1 produces cross-neutralizing antibodies against primary isolates with a matching narrow-neutralization sequence motif. *J. Virol.* **80**, 5552–5562
28. Matsushita, S., Takahama, S., Shibata, J., Kimura, T., Shiozaki, K., Eda, Y., Koito, A., Murakami, T., and Yoshimura, K. (2005) Ex vivo neutralization of HIV-1 quasi-species by a broadly reactive humanized monoclonal antibody KD-247. *Hum. Antibodies* **14**, 81–88
29. Eda, Y., Murakami, T., Ami, Y., Nakasone, T., Takizawa, M., Someya, K., Kaizu, M., Izumi, Y., Yoshino, N., Matsushita, S., Higuchi, H., Matsui, H., Shinohara, K., Takeuchi, H., Koyanagi, Y., Yamamoto, N., and Honda, M. (2006) Anti-V3 humanized antibody KD-247 effectively suppresses ex vivo generation of human immunodeficiency virus type 1 and affords sterile protection of monkeys against a heterologous simian/human immunodeficiency virus infection. *J. Virol.* **80**, 5563–5570
30. Murakami, T., Eda, Y., Nakasone, T., Ami, Y., Someya, K., Yoshino, N., Kaizu, M., Izumi, Y., Matsui, H., Shinohara, K., Yamamoto, N., and Honda, M. (2009) Postinfection passive transfer of KD-247 protects against simian/human immunodeficiency virus–induced $CD4^+$ T-cell loss in macaque lymphoid tissue. *AIDS* **23**, 1485–1494
31. Pflugrath, J. W. (1999) The finer things in X-ray diffraction data collection. *Acta Crystallogr. D Biol. Crystallogr.* **55**, 1718–1725
32. Matthews, B. W. (1985) Determination of protein molecular weight, hydration, and packing from crystal density. *Methods Enzymol.* **114**, 176–187
33. Vagin, A., and Teplyakov, A. (1997) MOLREP: an automated program for molecular replacement. *J. Appl. Cryst.* **30**, 1022–1025
34. Adams, P. D., Afonine, P. V., Bunkóczi, G., Chen, V. B., Davis, I. W., Echols, N., Headd, J. J., Hung, L. W., Kapral, G. J., Grosse-Kunstleve, R. W., McCoy, A. J., Moriarty, N. W., Oeffner, R., Read, R. J., Richardson, D. C., Richardson, J. S., Terwilliger, T. C., and Zwart, P. H. (2010) PHENIX: a comprehensive Python-based system for macromolecular structure solution. *Acta Crystallogr. D Biol. Crystallogr.* **66**, 213–221
35. Langer, G., Cohen, S. X., Lamzin, V. S., and Perrakis, A. (2008) Automated macromolecular model building for X-ray crystallography using ARP/wARP version 7. *Nat. Protoc.* **3**, 1171–1179
36. Murshudov, G. N., Vagin, A. A., and Dodson, E. J. (1997) Refinement of macromolecular structures by the maximum-likelihood method. *Acta Crystallogr. D Biol. Crystallogr.* **53**, 240–255
37. Emsley, P., Lohkamp, B., Scott, W. G., and Cowtan, K. (2010) Features and development of Coot. *Acta Crystallogr. D Biol. Crystallogr.* **66**, 486–501
38. Ong, Y. T., Kirby, K. A., Hachiya, A., Chiang, L. A., Marchand, B., Yoshimura, K., Murakami, T., Singh, K., Matsushita, S., and Sarafianos, S. G. (2012) Preparation of biologically active single-chain variable antibody fragments that target the HIV-1 gp120 V3 loop. *Cell. Mol. Biol. (Noisy-le-grand)* **58**, 71–79
39. Sreerama, N., and Woody, R. W. (1993) A self-consistent method for the analysis of protein secondary structure from circular dichroism. *Anal. Biochem.* **209**, 32–44

40. Sreerama, N., Venyaminov, S. Y., and Woody, R. W. (1999) Estimation of the number of alpha-helical and beta-strand segments in proteins using circular dichroism spectroscopy. *Protein Sci.* **8**, 370–380
41. Andrade, M. A., Chacón, P., Merelo, J. J., and Morán, F. (1993) Evaluation of secondary structure of proteins from UV circular dichroism spectra using an unsupervised learning neural network. *Protein Eng.* **6**, 383–390
42. Whitmore, L., and Wallace, B. A. (2004) DICHROWEB, an online server for protein secondary structure analyses from circular dichroism spectroscopic data. *Nucleic Acids Res.* **32**, W668-73
43. Whitmore, L., and Wallace, B. A. (2008) Protein secondary structure analyses from circular dichroism spectroscopy: methods and reference databases. *Biopolymers* **89**, 392–400
44. Janes, R. W. (2009) Reference datasets for protein ciruclar dichroism and synchrotron radiation circular dichroism spectroscopic analyses. In *Modern Techniques in Circular Dichroism and Synchrotron Radiation Circular Dichroism Spectroscopy*, Vol. 1, *Advances in Biomedical Spectroscopy* (Wallace, B. A., and Janes, R. W., eds.), pp. 183–201, IOS Press, Amsterdam, Netherlands
45. Shaw, G. M., Hahn, B. H., Arya, S. K., Groopman, J. E., Gallo, R. C., and Wong-Staal, F. (1984) Molecular characterization of human T-cell leukemia (lymphotropic) virus type III in the acquired immune deficiency syndrome. *Science* **226**, 1165–1171
46. Gallo, R. C., Salahuddin, S. Z., Popovic, M., Shearer, G. M., Kaplan, M., Haynes, B. F., Palker, T. J., Redfield, R., Oleske, J., Safai, B., et al. (1984) Frequent detection and isolation of cytopathic retroviruses (HTLV-III) from patients with AIDS and at risk for AIDS. *Science* **224**, 500–503
47. Montefiori, D. C. (2009) Measuring HIV neutralization in a luciferase reporter gene assay. *Methods Mol. Biol.* **485**, 395–405
48. Chen, V. B., Arendall III, W. B., Headd, J. J., Keedy, D. A., Immormino, R. M., Kapral, G. J., Murray, L. W., Richardson, J. S., and Richardson, D. C. (2010) MolProbity: all-atom structure validation for macromolecular crystallography. *Acta Crystallogr. D Biol. Crystallogr.* **66**, 12–21
49. Ramachandran, G. N., and Sasisekharan, V. (1968) Conformation of polypeptides and proteins. *Adv. Protein Chem.* **23**, 283–437
50. Stanfield, R. L., Zemla, A., Wilson, I. A., and Rupp, B. (2006) Antibody elbow angles are influenced by their light chain class. *J. Mol. Biol.* **357**, 1566–1574
51. Kabat, E. A., Wu, T. T., Perry, H. M., Gottesman, K. S., and Foeller, C. (1991) *Sequences of Proteins of Immunological Interest*, National Institutes of Health, Bethesda, MD
52. Abhinandan, K. R., and Martin, A. C. (2008) Analysis and improvements to Kabat and structurally correct numbering of antibody variable domains. *Mol. Immunol.* **45**, 3832–3839
53. Al-Lazikani, B., Lesk, A. M., and Chothia, C. (1997) Standard conformations for the canonical structures of immunoglobulins. *J. Mol. Biol.* **273**, 927–948
54. Shirai, H., Kidera, A., and Nakamura, H. (1996) Structural classification of CDR-H3 in antibodies. *FEBS Lett.* **399**, 1–8
55. Stanfield, R. L., Ghiara, J. B., Ollmann Saphire, E., Profy, A. T., and Wilson, I. A. (2003) Recurring conformation of the human immunodeficiency virus type 1 gp120 V3 loop. *Virology* **315**, 159–173
56. Ratner, L., Fisher, A., Jagodzinski, L. L., Mitsuya, H., Liou, R. S., Gallo, R. C., and Wong-Staal, F. (1987) Complete nucleotide sequences of functional clones of the AIDS virus. *AIDS Res. Hum. Retroviruses* **3**, 57–69
57. Javaherian, K., Langlois, A. J., LaRosa, G. J., Profy, A. T., Bolognesi, D. P., Herlihy, W. C., Putney, S. D., and Matthews, T. J. (1990) Broadly neutralizing antibodies elicited by the hypervariable neutralizing determinant of HIV-1. *Science* **250**, 1590–1593
58. Bell, C. H., Pantophlet, R., Schiefner, A., Cavacini, L. A., Stanfield, R. L., Burton, D. R., and Wilson, I. A. (2008) Structure of antibody F425-B4e8 in complex with a V3 peptide reveals a new binding mode for HIV-1 neutralization. *J. Mol. Biol.* **375**, 969–978
59. Burke, V., Williams, C., Sukumaran, M., Kim, S. S., Li, H., Wang, X. H., Gorny, M. K., Zolla-Pazner, S., and Kong, X. P. (2009) Structural basis of the cross-reactivity of genetically related human anti-HIV-1 mAbs: implications for design of V3-based immunogens. *Structure* **17**, 1538–1546
60. Jiang, X., Burke, V., Totrov, M., Williams, C., Cardozo, T., Gorny, M. K., Zolla-Pazner, S., and Kong, X. P. (2010) Conserved structural elements in the V3 crown of HIV-1 gp120. *Nat. Struct. Mol. Biol.* **17**, 955–961
61. Stanfield, R. L., Gorny, M. K., Williams, C., Zolla-Pazner, S., and Wilson, I. A. (2004) Structural rationale for the broad neutralization of HIV-1 by human monoclonal antibody 447-52D. *Structure* **12**, 193–204
62. Yoshimura, K., Shibata, J., Kimura, T., Honda, A., Maeda, Y., Koito, A., Murakami, T., Mitsuya, H., and Matsushita, S. (2006) Resistance profile of a neutralizing anti-HIV monoclonal antibody, KD-247, that shows favourable synergism with anti-CCR5 inhibitors. *AIDS* **20**, 2065–2073
63. Hatada, M., Yoshimura, K., Harada, S., Kawanami, Y., Shibata, J., and Matsushita, S. (2010) Human immunodeficiency virus type 1 evasion of a neutralizing anti-V3 antibody involves acquisition of a potential glycosylation site in V2. *J. Gen. Virol.* **91**, 1335–1345
64. Kessler, N., Zvi, A., Ji, M., Sharon, M., Rosen, O., Levy, R., Gorny, M., Zolla-Pazner, S., and Anglister, J. (2003) Expression, purification, and isotope labeling of the Fv of the human HIV-1 neutralizing antibody 447-52D for NMR studies. *Protein Expr. Purif.* **29**, 291–303
65. Brändén, C., and Tooze, J. (1999) *Introduction to Protein Structure*, Garland Science, New York
66. Greenfield, N., and Fasman, G. D. (1969) Computed circular dichroism spectra for the evaluation of protein conformation. *Biochemistry* **8**, 4108–4116
67. Eglen, R. M., Reisine, T., Roby, P., Rouleau, N., Illy, C., Bossé, R., and Bielefeld, M. (2008) The use of AlphaScreen technology in HTS: current status. *Curr. Chem. Genomics* **1**, 2–10
68. Sundberg, E. J. (2009) Structural basis of antibody-antigen interactions. *Methods Mol. Biol.* **524**, 23–36
69. Stanfield, R. L., Gorny, M. K., Zolla-Pazner, S., and Wilson, I. A. (2006) Crystal structures of human immunodeficiency virus type 1 (HIV-1) neutralizing antibody 2219 in complex with three different V3 peptides reveal a new binding mode for HIV-1 cross-reactivity. *J. Virol.* **80**, 6093–6105
70. Gorny, M. K., Xu, J. Y., Karwowska, S., Buchbinder, A., and Zolla-Pazner, S. (1993) Repertoire of neutralizing human monoclonal antibodies specific for the V3 domain of HIV-1 gp120. *J. Immunol.* **150**, 635–643
71. Julien, J. P., Cupo, A., Sok, D., Stanfield, R. L., Lyumkis, D., Deller, M. C., Klasse, P. J., Burton, D. R., Sanders, R. W., Moore, J. P., Ward, A. B., and Wilson, I. A. (2013) Crystal structure of a soluble cleaved HIV-1 envelope trimer. *Science* **342**, 1477–1483
72. Gorny, M. K., Revesz, K., Williams, C., Volsky, B., Louder, M. K., Anyangwe, C. A., Krachmarov, C., Kayman, S. C., Pinter, A., Nadas, A., Nyambi, P. N., Mascola, J. R., and Zolla-Pazner, S. (2004) The v3 loop is accessible on the surface of most human immunodeficiency virus type 1 primary isolates and serves as a neutralization epitope. *J. Virol.* **78**, 2394–2404

Received for publication June 6, 2014.
Accepted for publication August 26, 2014.

Journal of General Virology (2014), 95, 1816–1826 DOI 10.1099/vir.0.062885-0

Impact of maraviroc-resistant and low-CCR5-adapted mutations induced by *in vitro* passage on sensitivity to anti-envelope neutralizing antibodies

Kazuhisa Yoshimura,[1,2]† Shigeyoshi Harada,[1,2]† Samatchaya Boonchawalit,[1,2] Yoko Kawanami[2] and Shuzo Matsushita[2]

Correspondence
Kazuhisa Yoshimura
ykazu@nih.go.jp
Shuzo Matsushita
shuzo@kumamoto-u.ac.jp

[1]AIDS Research Centre, National Institute of Infectious Diseases, 1-23-1 Toyama, Shinjuku-ku, Tokyo 162-8640, Japan

[2]Center for AIDS Research, Kumamoto University, 2-2-1 Honjo, Chuo-ku, Kumamoto 860-0811, Japan

The aim of this study was to generate maraviroc (MVC)-resistant viruses *in vitro* using a human immunodeficiency virus type 1 subtype B clinical isolate (HIV-1_{KP-5}) to understand the mechanism(s) of resistance to MVC. To select HIV-1 variants resistant to MVC *in vitro*, we exposed high-chemokine (C-C motif) receptor 5 (CCR5)-expressing PM1/CCR5 cells to HIV-1_{KP-5} followed by serial passage in the presence of MVC. We also passaged HIV-1_{KP-5} in PM1 cells, which were low CCR5 expressing to determine low-CCR5-adapted substitutions and compared the Env sequences of the MVC-selected variants. Following 48 passages with MVC (10 μM), HIV-1_{KP-5} acquired a resistant phenotype [maximal per cent inhibition (MPI) 24 %], whilst the low-CCR5-adapted variant had low sensitivity to MVC (IC_{50} ~200 nM), but not reduction of the MPI. The common substitutions observed in both the MVC-selected and low-CCR5-adapted variants were selected from the quasi-species, in V1, V3 and V5. After 14 passages, the MVC-selected variants harboured substitutions around the CCR5 N-terminal-binding site and V3 (V200I, T297I, K305R and M434I). The low-CCR5-adapted infectious clone became sensitive to anti-CD4bs and CD4i mAbs, but not to anti-V3 mAb and autologous plasma IgGs. Conversely, the MVC-selected clone became highly sensitive to the anti-envelope (Env) mAbs tested and the autologous plasma IgGs. These findings suggest that the four MVC-resistant mutations required for entry using MVC-bound CCR5 result in a conformational change of Env that is associated with a phenotype sensitive to anti-Env neutralizing antibodies.

Received 15 December 2013
Accepted 29 April 2014

INTRODUCTION

Human immunodeficiency virus type 1 (HIV-1) entry into target cells is triggered by the interaction of the viral envelope glycoproteins (Env) with its receptor CD4 and one or two major coreceptors, chemokine (C-C motif) receptor 5 (CCR5) or chemokine (C-X-C motif) receptor 4 (CXCR4), and culminates in fusion of the viral and cell membranes. Env is organized into trimers on virions, and consists of the gp120 surface and gp41 transmembrane subunits (Wyatt & Sodroski, 1998). The small-molecule CCR5 antagonist maraviroc (MVC) was the first CCR5 inhibitor licensed for clinical use (Gulick *et al.*, 2008). CCR5 inhibitors work by allosterically altering the conformation of CCR5 at the cell surface, thereby disrupting its interaction with HIV gp120 (Berger *et al.*, 1999; Dorr *et al.*, 2005). Although MVC and another CCR5 inhibitor, vicriviroc (VCV), can efficiently suppress HIV-1 replication, resistant variants can arise both *in vitro* and *in vivo*, and these resistant viruses are adapted to use drug-bound CCR5 for entry (Berro *et al.*, 2009; Kuhmann *et al.*, 2004; Marozsan *et al.*, 2005; Ogert *et al.*, 2009, 2010; Ratcliff *et al.*, 2013; Roche *et al.*, 2011b; Tilton *et al.*, 2010; Tsibris *et al.*, 2008; Westby *et al.*, 2007; Yuan *et al.*, 2011; Yusa *et al.*, 2005). Current models of gp120 binding to a coreceptor suggest that the crown of the gp120 V3 loop interacts principally with the second extracellular loop region of the coreceptor, whilst the gp120 bridging sheet, which is formed after CD4 binding, and the stem of the V3 loop interact with the N terminus of the coreceptor (Brelot *et al.*, 1999; Cormier & Dragic, 2002; Farzan *et al.*, 1999; Huang *et al.*, 2005). The development of resistance is an important issue for HIV treatment regimens incorporating MVC, as is the case for any antimicrobial agent.

†These authors contributed equally to this work.

The GenBank/EMBL/DDBJ accession numbers for the envelope sequences of KP-5 are AB742145–AB742157.

Three supplementary figures are available with the online version of this paper.

HIV-1 can develop clinical resistance to CCR5 antagonists by two routes. The first pathway is through emergence of pre-existing CXCR4-using viruses (Fätkenheuer *et al.*, 2008; Landovitz *et al.*, 2008; Westby *et al.*, 2006). CCR5 inhibitor evasion can also occur by the accumulation of multiple mutations in gp120 and/or gp41 without a switch in coreceptor usage (Dragic *et al.*, 2000; Maeda *et al.*, 2006, 2008a; Roche *et al.*, 2011b; Tsamis *et al.*, 2003). The resistant pathway is characterized not by shifts in IC_{50} (a competitive inhibitor), but rather by reductions in the maximal per cent inhibition (MPI). Reductions in MPI are due to the resistant virus developing the ability to bind to the antagonist-modified form of CCR5 (Westby *et al.*, 2007). However, one study reported that chimeric clones bearing the N425K mutation in C4 replicated at high MVC concentrations and displayed significant shifts in IC_{50}s, characteristic of resistance to all other antiretroviral drugs, but not MVC (Ratcliff *et al.*, 2013).

Escape mutants to the CCR5 inhibitor, AD101 (SCH-350581), have been found to be more sensitive than the parental isolate to a subset of neutralizing mAbs against V3 and a CD4-induced (CD4i) epitope (Pugach *et al.*, 2007; Berro *et al.*, 2009). To date, however, it is not clear which mutation(s) induced by MVC affect the accessibility of neutralizing mAbs to the epitopes in Env.

Therefore, to determine the resistance mechanisms to MVC, we passaged a primary CCR5-tropic (R5) subtype B isolate in the high-CCR5-expressing T-cell line PM1/CCR5 in the presence of MVC (Fig. S1, available in the online Supplementary Material) and compared the Env sequences of variants with those cultured in the low-CCR5-expressing parental PM1 cell line (Fig. S1). We also investigated the phenotypic change in the MVC-resistant clone against anti-Env antibodies, especially for anti-V3 neutralizing mAbs and autologous plasma IgGs, and compared the results with the low-CCR5-adapted clone to determine the key mutations for accessibility of neutralizing mAbs to the epitopes in Env.

RESULTS

Anti-HIV-1 activities of MVC toward laboratory strains and primary HIV-1 isolates

Initially, we determined the MPI and the IC_{50} values of MVC against different laboratory-adapted and primary HIV-1 isolates, including both CXCR4-tropic (X4) and R5 viruses. MVC inhibited the laboratory-adapted HIV-1 R5 strains HIV-1_{BaL} and HIV-$1_{JR\text{-}FL}$ with MPIs of 98 and 97 %, respectively, but did not inhibit the X4 virus HIV-1_{IIIB} or dual-tropic virus HIV-$1_{89.6}$ (MPI <20 %, Table 1). We also tested MVC against 14 R5 primary isolates, including subtypes B, C and G, and the circulating recombinant form CRF08_BC. MVC effectively inhibited all of these primary isolates at concentrations of 1.2–26 nM (MPI 92–100 %), but did not inhibit three primary X4 isolates (two CRF01_AE and one subtype B) with MPI <20 % (Table 1).

Table 1. Inhibitory activities of MVC toward infection by laboratory-adapted and primary strains of HIV-1

Virus	Subtype	IC_{50}* (nM)	MPI (%)
Laboratory adapted			
R5			
HIV-1_{BaL}	B	26	98
HIV-$1_{JR\text{-}FL}$	B	6.9	97
Dual			
HIV-$1_{89.6}$	B	>1000	<20
X4			
HIV-1_{IIIB}	B	>1000	<20
Primary			
R5			
HIV-$1_{KP\text{-}5}$	B	26	92
HIV-$1_{KP\text{-}2}$	CRF08_BC	24	95
HIV-$1_{KP\text{-}6}$	G	20	95
HIV-$1_{KP\text{-}7}$	B	18	95
HIV-$1_{KP\text{-}8}$	B	14	97
HIV-$1_{KP\text{-}9}$	B	13	96
HIV-$1_{KP\text{-}10}$	B	9.2	98
HIV-$1_{KP\text{-}11}$	C	8.6	96
HIV-$1_{KP\text{-}12}$	B	5.1	98
HIV-$1_{KP\text{-}13}$	B	4.0	96
HIV-$1_{KP\text{-}14}$	B	3.0	95
HIV-$1_{KP\text{-}15}$	B	3.0	94
HIV-$1_{KP\text{-}16}$	B	2.2	100
HIV-$1_{KP\text{-}17}$	B	1.2	98
X4/mix			
HIV-$1_{KP\text{-}18}$	CRF01_AE	>1000	<20
HIV-$1_{KP\text{-}19}$	CRF01_AE	>1000	<20
HIV-$1_{KP\text{-}20}$	B	>1000	<20

*PM1/CCR5 cells (2×10^3) were exposed to 100 $TCID_{50}$ of each virus and then cultured in the presence of various concentrations of MVC. The IC_{50} values were determined by the WST-8 assay using a Cell Counting kit-8 on day 7 of culture. All assays were conducted in duplicate or triplicate.

Selection of MVC-resistant variants

To select MVC-resistant HIV-1 variants *in vitro*, we exposed PM1/CCR5 cells to HIV-$1_{KP\text{-}5}$, which had the highest IC_{50} value (26 nM) and lowest MPI (92 %) among the primary isolates tested, and serially passaged the viruses in the presence of increasing concentrations of MVC. As a control, HIV-$1_{KP\text{-}5}$ was passaged under the same conditions without MVC in PM1/CCR5 cells (designated the passage control). Moreover, to compare the differences between the MVC-resistant variant and low-CCR5-expressing-cell-adapted variant, we passaged HIV-$1_{KP\text{-}5}$ in low-CCR5-expressing parental PM1 cells (designated low-CCR5-adapted). The selected virus was initially propagated in the presence of 1 nM MVC and during the course of the selection procedure the concentration of MVC was increased to 10 μM over 48 passages (Fig. 1a).

Resistance to small-molecule CCR5 inhibitors is known to vary according to the cell type used (Anastassopoulou

et al., 2009; Ogert *et al.*, 2008; Pugach *et al.*, 2007; Westby *et al.*, 2007). To characterize the resistance profiles of the passaged variants, we tested the sensitivities of the three variants and HIV-1_{BaL} to MVC in phytohaemagglutinin (PHA)-activated PBMCs (Fig. 1b). The MPI of the MVC-resistant variant was lower than the MPIs of the passage control, low-CCR5-adapted variant and HIV-1_{BaL} (MPI 80.3 versus 92.3, 94.5 and 95.7 %, respectively).

The MVC-selected variant became highly resistant to MVC (Fig. 2), with an MPI of 24 % at 48 passages. However, the low-CCR5-adapted variant, which was passaged in PM1 cells, became low sensitive to MVC compared with the passage control (IC_{50} 279 versus 26.3 nM), but we did not find a reduction in the MPI.

We also determined the sequential MPIs and IC_{50} values of each passaged variant to MVC (Fig. 2). From passages

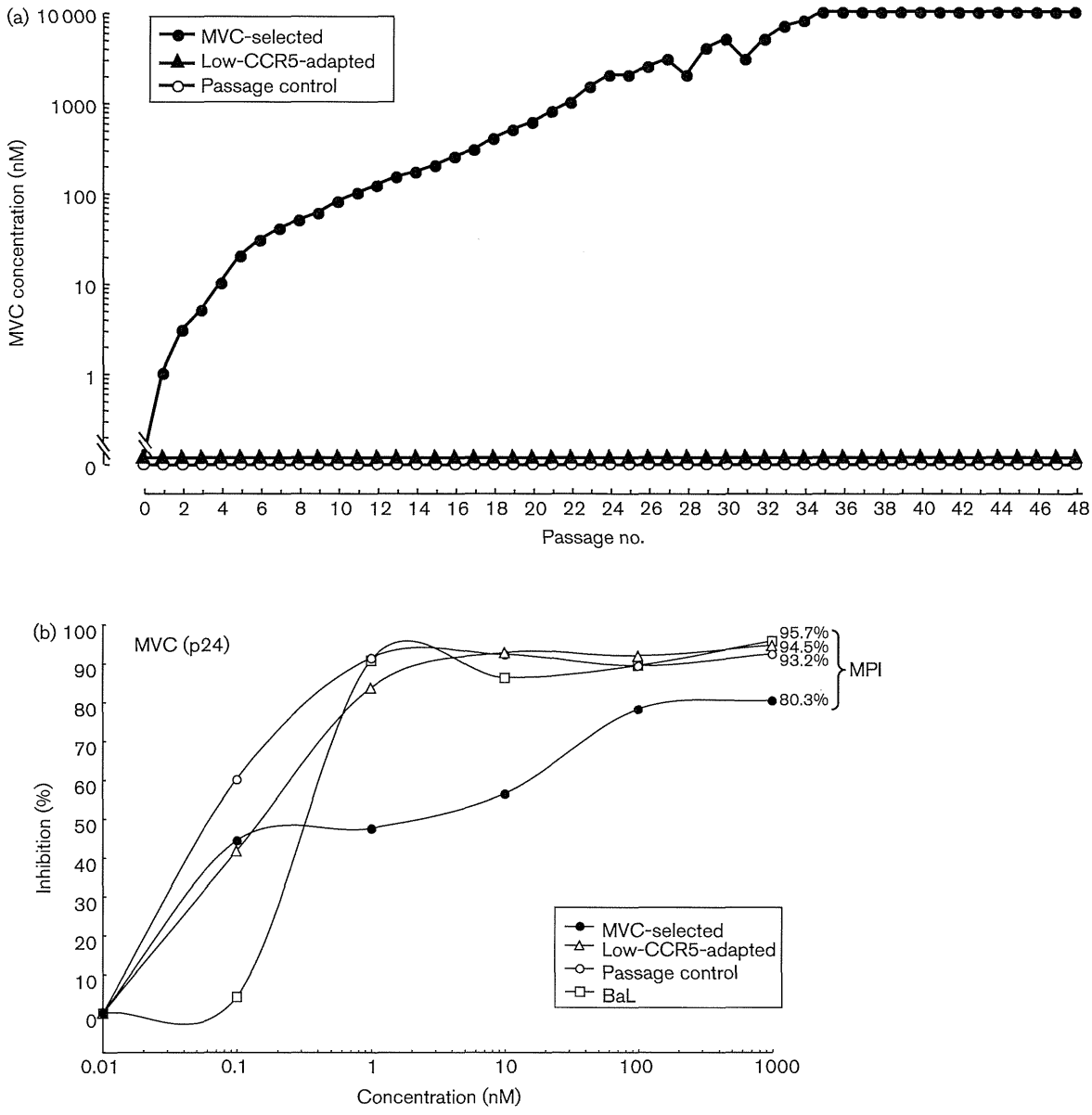

Fig. 1. Selection of MVC-resistant and low-CCR5-adapted virus variants. (a) The selection was carried out in PM1/CCR5 and PM1 cells as described in Methods. (b) Sensitivities of the MVC-selected (48 passages), low-CCR5-adapted (48 passages), passage control (48 passages) variants and HIV-1_{BaL} (BaL) to MVC as determined by p24 antigen measurement. PHA-activated PBMCs (1×10^6 cells ml^{-1}) were exposed to 100 $TCID_{50}$ of each variant and cultured in the presence or absence of various concentrations of the drug in 96-well microculture plates. The amounts of p24 antigen produced by the cells were determined on day 7. All assays were performed in triplicate.